

SKI Report 2003:28  
SSI report 2003:11

Research

---

## **AMBER and Ecolego Intercomparisons using Calculations from SR 97**

Philip Maul  
Peter Robinson  
Rodolfo Avila  
Robert Broed  
António Pereira  
Shulan Xu

August 2003

ISSN 1104-1374  
ISSN 0282-4434  
ISRN SKI-R-03/28-SE



## **SKI/SSI perspective**

### **Background**

As part of preparations for review of future license applications, the Swedish Nuclear Power Inspectorate (SKI) and Swedish Radiation Protection Authority (SSI) are developing their capabilities of doing radionuclide transport calculation. For this purpose SKI and SSI have developed the software program AMBER and Ecolego respectively.

The AMBER compartmental modelling software has been used by Quintessa in undertaking Performance Assessment (PA) calculations for SKI for the last four years. In particular, it was used in helping to identify key issues in the safety case for SFR 1. SSI and the Norwegian Radiation Protection Authority (NRPA) are supporting the development of Ecolego which is based on the Matlab/Simulink general purpose modelling software and provides a user-friendly Graphical User Interface (GUI) which is particularly suitable for undertaking PA calculations.

### **Purpose of the project**

The purpose of this project is to undertake some intercomparison calculations using AMBER and Ecolego based on calculation cases considered in SR 97. The reasons for undertaking such intercomparisons are to give confidence in the use of AMBER and Ecolego for whole system PA calculations for a deep repository and to provide SKI and SSI with an understanding of some of the technical issues raised by seeking to repeat the SR 97 calculations with different models and software.

### **Results**

The objective of this project has as a whole been fulfilled. There is good agreement between the two modelling software. In several instances the SR 97 documentation was not sufficiently clear to enable the implementation of the SKB models in AMBER and Ecolego to be unambiguous.

### **Project information**

SKI project manager: Benny Sundström.

Project identification number: 14.9-030741/03138

SSI project manager: Shulan Xu.

#### *Relevant report:*

Radionuclide Transport Modelling: Current Status and Future Needs - Seminar  
Johannesberg, Sweden, 6-8 November 2001 Synthesis, Work Group Reports and  
Extended Abstracts, Swedish Nuclear Power Inspectorate, Stockholm, Sweden, 2002.



## Research

---

# AMBER and Ecolego Intercomparisons using Calculations from SR 97

Philip Maul<sup>1</sup>  
Peter Robinson<sup>1</sup>  
Rodolfo Avila<sup>2</sup>  
Robert Broed<sup>3</sup>  
António Pereira<sup>3</sup>  
Shulan Xu<sup>4</sup>

<sup>1</sup>Quintessa Limited, Dalton House, Newtown Road, Henley-on-Thames,  
Oxfordshire RG9 1HG, United Kingdom

<sup>2</sup>Facilia AB, Valsgärdevägen 12, SE-168 53 Bromma, Stockholm, Sweden

<sup>3</sup>Department of Physics, Center of Physics, Astronomy and Biotechnology,  
AlbaNova University Center, Stockholm University, SE-106 91 Stockholm, Sweden

<sup>4</sup>Swedish Radiation Protection Authority, SE-171 16 Stockholm, Sweden

August 2003

This report concerns a study which has been conducted for the Swedish Nuclear Power Inspectorate (SKI) and the Swedish Radiation Protection Authority (SSI). The conclusions and viewpoints presented in the report are those of the author/authors and do not necessarily coincide with those of the SKI and the SSI.



## Summary

The AMBER compartmental modelling software has been used by Quintessa in undertaking Performance Assessment (PA) calculations for SKI for the last four years. In particular, it was used in helping to identify key issues in the safety case for SFR 1. SSI and the Norwegian Radiation Protection Authority (NRPA) are supporting the development of Ecolego which is based on the Matlab/Simulink general purpose modelling software and provides a user-friendly Graphical User Interface (GUI) which is particularly suitable for undertaking PA calculations.

At SKI/SSI expert group meetings in September 2002, Quintessa presented some radionuclide transport calculations for a deep repository for spent fuel using AMBER. Comparisons were presented with calculations undertaken by SKB in their SR 97 study. It was agreed that it would be useful to undertake some intercomparison calculations using AMBER and Ecolego based on calculation cases considered in SR 97. The reasons for undertaking such intercomparisons include:

1. to give confidence in the use of AMBER and Ecolego for whole system PA calculations for a deep repository; and
2. to provide SKI and SSI with an understanding of some of the technical issues raised by seeking to repeat the SR 97 calculations with different models and software.

This report documents the intercomparison calculations that have been undertaken. The main conclusions that have been drawn are:

1. Both modelling packages could successfully reproduce SKB's SR 97 calculations for the near field, geosphere and biosphere.
2. The results of the deterministic calculations for the near field and both deterministic and probabilistic calculations for the biosphere, where AMBER and Ecolego used compartment models, were typically in agreement to within one significant figure. The identical results for the calculated equilibrium inventories in Bay sediments illustrate that the calculations by AMBER and Ecolego are essentially the same when the compartment models are identical. The residual differences in the other calculations are due to small differences in the interpretation of the SR 97 models and data.
3. The results of the deterministic calculations for the geosphere, where AMBER used a compartment model and Ecolego a one-dimensional contaminant transport model, were also generally in agreement to within one significant figure, except where radionuclides fluxes are very low (e.g., for  $^{239}\text{Pu}$ ), where the compartmental approximation in AMBER can overestimate the output flux.
4. In several instances the SR 97 documentation was not sufficiently clear to enable the implementation of the models in AMBER and Ecolego to be unambiguous. Examples include the structure of the coastal biosphere model and the algorithms used in some of the dose calculations.

5. Some key issues for the SR 97 assessment have been identified; these provide an indication of where detailed scrutiny will be required of any safety case made by SKB for a deep repository.

# Sammanfattning

Mjukvaran för kompartmentmodellen AMBER har använts av Quintessa i säkerhetsanalysberäkningar för SKI under de senaste fyra åren. Speciellt har AMBER använts i identifieringen av nyckelfrågor i säkerhetsredovisning för SFR 1. SSI och statens strålevern i Norge stöder utvecklingen av Ecolego vilken är baserad på den kommersiella programvaran Matlab/Simulink. Ecolego har ett användarvänligt grafiskt gränssnitt vilken särskilt lämpar sig för säkerhetsanalysberäkningar.

Vid ett SKI/SSI-expertgruppsmöte i september 2002 presenterade Quintessa några radionuklidberäkningar för ett djupförvar för använt kärnbränsle med hjälp av AMBER. Jämförelser med radionuklidberäkningar utförda av SKB i deras säkerhetsanalys SR 97 ingick också i Quintessa:s presentation. Vid mötet bestämde man att en beräkningsjämförelse mellan AMBER och Ecolego skulle vara värdefullt och då baserat på beräkningar gjorda i SR 97. Anledningen till en sådan jämförelse omfattar då:

1. att ge tillit i användandet av AMBER:s och Ecolego:s hela system för säkerhetsanalysberäkningar för ett djupförvar; och
2. att ge SKI och SSI kunskap om några av de tekniska frågeställningar som kan uppkomma när man försöker att upprepa SR 97 beräkningar med olika modeller och programvaror.

Denna rapport dokumentera dessa gjorda jämförande beräkningar. De huvudslutsatser som man kan dra är:

1. Båda modellpaketen kunde framgångsrikt reproducera SKB:s SR 97 beräkningar för närområdet, geosfären och biosfären.
2. Resultaten av de deterministiska beräkningarna för närområdet och de deterministiska och probabilistiska beräkningarna för biosfären, då AMBER och Ecolego använde kompartmentmodellerna, var typiskt inom en signifikant siffra. De identiska resultaten för de beräknade jämvikten av radionuklider i sediment för en havsvik illustrerar att beräkningarna med hjälp av AMBER och Ecolego är i huvudsak samma när kompartmentmodellerna är identiska. De resterande olikheterna i övriga beräkningar härrör sig från små olikheter i tolkningen av modeller och data i SR 97.
3. Resultaten från de deterministiska beräkningarna för geosfären, där AMBER använder kompartmentmodellering och Ecolego en endimensionell transportmodell, var också i allmänhet i överenskommelse med varandra inom en signifikant siffra. Ett undantag är då flödet av radionuklider är mycket litet (t.ex. för  $^{239}\text{Pu}$ ), vilken leder till att AMBER kan ge ett för högt flöde ut från geosfären.
4. I flera fall var dokumentationen i SR 97 inte tillräcklig tydlig för att entydigt kunna utnyttja modellerna i AMBER och Ecolego. Exempel på detta är strukturen på modellen för biosfären för kustområdet och de algoritmer som används vid några av dosberäkningarna.

5. Några nyckelfrågor i SR 97-analysen har identifierats; dessa ger en indikation på var en noggrann undersökning behövs i kommande säkerhetsanalyser utförda av SKB för ett djupförvar.

# Contents

<b>1</b>	<b>INTRODUCTION .....</b>	<b>1</b>
<b>2</b>	<b>CASE 1: THE MAIN DETERMINISTIC TEST CASE .....</b>	<b>3</b>
2.1	THE NEAR FIELD .....	3
2.1.1	<i>Test Case Specification</i> .....	3
2.1.2	<i>Intercomparisons</i> .....	11
2.2	THE GEOSPHERE .....	16
2.2.1	<i>Test Case Specification</i> .....	16
2.2.2	<i>The Representation of the Geosphere in AMBER</i> .....	18
2.2.3	<i>The Representation of the Geosphere in Ecolego</i> .....	19
2.2.4	<i>Intercomparisons</i> .....	21
2.3	THE BIOSPHERE .....	27
2.3.1	<i>Test Case Specification</i> .....	27
2.3.2	<i>Intercomparisons</i> .....	31
2.4	SENSITIVITY CALCULATIONS .....	34
<b>3</b>	<b>CASE 2: A SIMPLE PROBABILISTIC TEST CASE.....</b>	<b>37</b>
3.1	TEST CASE SPECIFICATION .....	37
3.2	INTERCOMPARISONS .....	37
<b>4</b>	<b>CASE 3: VARIATIONS ON CASE 1 .....</b>	<b>43</b>
4.1	TEST CASE 3.1 .....	43
4.1.1	<i>Test Case Specification</i> .....	43
4.1.2	<i>Intercomparisons</i> .....	43
4.2	TEST CASE 3.2 .....	47
4.2.1	<i>Test Case Specification</i> .....	47
4.2.2	<i>Intercomparisons</i> .....	47
<b>5</b>	<b>CONCLUSIONS.....</b>	<b>51</b>
	<b>REFERENCES.....</b>	<b>53</b>



# 1 Introduction

The AMBER compartmental modelling software (Enviros QuantiSci and Quintessa Ltd, 2002) has been used by Quintessa in undertaking Performance Assessment (PA) calculations for SKI for the last four years. In particular, it was used in helping to identify key issues in the safety case for SFR 1 (Maul and Robinson, 2002).

SSI the Norwegian Radiation Protection Authority (NRPA) are supporting the development of Ecolego (Avilia et al., 2003) which is based on the Matlab/Simulink general purpose modelling software and provides a user-friendly Graphical User Interface (GUI) which is particularly suitable for undertaking PA calculations.

At SKI/SSI expert group meetings in September 2002, Quintessa presented some radionuclide transport calculations for a deep repository for spent fuel using AMBER. Comparisons were presented with calculations undertaken by SKB in their SR 97 study (Lindgren and Lindström, 1999 and Hedin, 2002). It was agreed that it would be useful to undertake some intercomparison calculations using AMBER and Ecolego based on calculation cases considered in SR 97. The reasons for undertaking such intercomparisons include:

1. to give confidence in the use of AMBER and Ecolego for whole system PA calculations for a deep repository; and
2. to provide SKI and SSI with an understanding of some of the technical issues raised by seeking to repeat the SR 97 calculations with different models and software.

This report provides details of the intercomparison test cases and the results obtained using AMBER and Ecolego. Some additional related calculations have been undertaken:

- Quintessa has used the Matlab/Simulink software directly (separately from Ecolego) for some SR 97 calculation cases. This has proved useful in demonstrating some of the capabilities of these general-purpose modelling packages for PA calculations, and provided additional confirmation of the validity of some AMBER calculations. This work is, however, not part of the AMBER/Ecolego intercomparisons, and will be reported separately.
- Additional AMBER/Ecolego intercomparisons are to be undertaken which are relevant to some capabilities not tested in the SR 97 calculations. Again, these comparisons are not included in the present report.

This report is structured as follows:

In Section 2 the main deterministic test case is presented, based on a chosen SR 97 calculation and involving near-field, geosphere and biosphere sub-models.

In Section 3 a simple probabilistic test case is presented; this uses the biosphere sub-model used in the main deterministic test case.

Section 4 describes near-field variants to the main deterministic test case of Section 2. The parameter variations considered are not necessarily realistic; the aim is simply to explore a wider range of calculations to test the two codes.

Finally, Section 5 summarises the main conclusions that can be drawn.

## 2 Case 1: The Main Deterministic Test Case

This test case is based on the SR 97 test calculations described in Section 4.2.1 of Lindgren and Lindström (1999), with the coastal biosphere described in Bergström et al. (1999). The details of each of the three sub-models and the calculations undertaken at each stage are given in the following sub-sections. Results are presented for selected radionuclides.

### 2.1 The Near Field

#### 2.1.1 Test Case Specification

Although Lindgren and Lindström (1999), Romero et al. (1999) and Lindgren and Widén (1998) describe the near-field compartment model used by SKB in some detail, the information provided is not always clear. For this reason the interpretation used by Quintessa is described in some detail here; some of the details may differ slightly from the actual SKB implementation.

Figure 3.2 of Lindgren and Lindström (1999) shows the block structure and the compartments used, and the same nomenclature will be used here. Table 2.1.1 and Figure 2.1.1 give details of the blocks used, some of which are broken down into a number of compartments. Table 2.1.2 gives the release pathways from the near field to the geosphere.

The data used in the SR 97 calculations are generally clearly specified in the SKB documents. Table 2.1.3 gives details of the data sources that have been used.

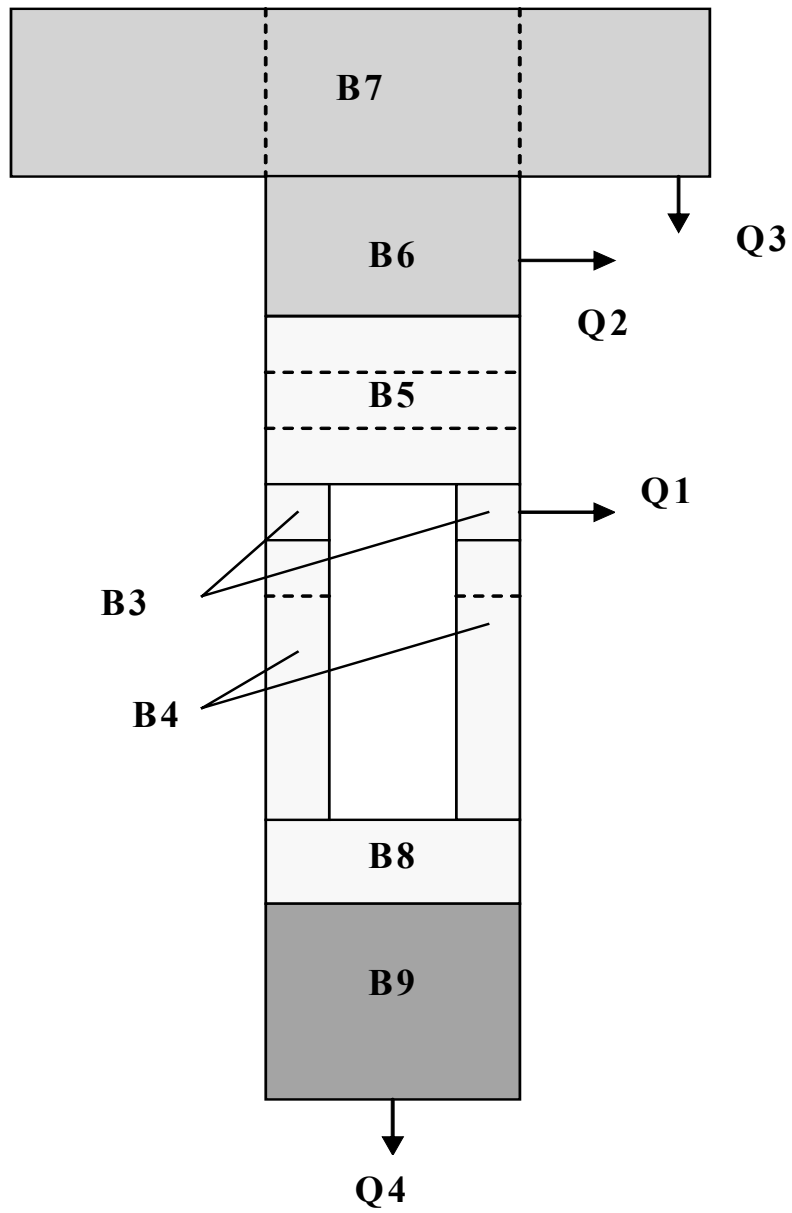


**Figure 2.1.1.** Discretisation of the Near Field (Based on Figure 24 of Lindgren et al., 1998).

**Table 2.1.1.** Near-Field Blocks.

Block	Description	Number of compartments	Comment
B1	inside the canister (water)	1	Not shown explicitly in Figure 2.1.1
B2	the hole in the canister (water)	1	Not shown explicitly in Figure 2.1.1
B3	the buffer next to the hole	6 annular compartments of equal thickness (0.058 m)	The height of these compartments is 0.5 m
B4	The rest of the buffer around the canister	2 annular compartments, each of the full thickness, one above the other	The upper compartment is 1.0 m high and the lower 3.33 m high
B5	The buffer above the canister	3 equal layers	The height of these compartments is 0.5 m
B6	The backfill at the top of the deposition hole	1	The height of this compartment is 1.0 m
B7	The tunnel backfill	3	The geometry is hard to understand. It has been assumed that each compartment has the full tunnel cross-section, with the centre one the width of the deposition hole (1.75 m) and the others 2.125 m wide (6 m in total)
B8	The buffer below the canister	1	The height of this compartment is 0.5 m
B9	Rock below the deposition hole	1	The height of this compartment is 3.0 m

**Table 2.1.2.** Near-Field Release Routes.

Route	Location
Q1	From the outer B3 compartment
Q2	From the B6 block
Q3	From one of the outer B7 compartments
Q4	From the rock below the deposition hole

**Table 2.1.3.** Near-Field Data Sources.

Parameter	Data Source
Canister Inventory	TR-99-23 Table 3-3 and Hedin (2002) Table II.
Instant Release Fractions	'Reasonable' values TR-99-23 Table 3-4 and Hedin (2002) Table II.
Fuel Dissolution Rate	$1\text{E-}8 \text{ y}^{-1}$ . Hedin (2002) Table I.
Number of defective canisters	5. Pessimistic estimate TR-99-23 Table 3-5
Elemental Solubilities	TR-99-23 Table 3-6 for Aberg
Canister hole area	Hedin (2002) Table I
Delay time before release commences	300 years. Pessimistic estimate TR-99-23 Table 3-5 and Hedin (2002) Table I.
Time when hole increases in size	20 000 years. Pessimistic estimate TR-99-23 Table 3-5 and Hedin (2002) Table I.
Effective diffusivities	TR-99-23 Table 3-4
Distribution coefficients	'Reasonable' values TR-99-23 Table 3-7.
Bentonite porosity and density	TR-99-23 Table 3-8

## Transfers between Near-Field Compartments

Diffusional transfers can take place in horizontal or vertical directions, and these have been specified by SKB in terms of resistances between compartments. For diffusion in a given direction, the resistance between compartments  $i$  and  $j$  is given by:

$$\Omega^{ij} = \frac{1}{2} \left( \frac{d^i}{D^i A^i} + \frac{d^j}{D^j A^j} \right), \quad (2.1)$$

where  $A$  is the area perpendicular to the direction of transport,  $D$  is the effective diffusion coefficient, and  $d$  is the length of the compartment in the direction of radionuclide transport.

It should be noted that other approaches are possible, particularly with regard to the representation of transport areas. For example, it can be argued that the following representation of the resistance would be preferable:

$$\Omega^{ij} = \frac{1}{2 A^{ij}} \left( \frac{d^i}{D^i} + \frac{d^j}{D^j} \right), \quad (2.2)$$

where  $A^{ij}$  is the common area between the two compartments. Additional, variant, calculations have been undertaken with this different representation, but, as indicated by Hedin (2002), for the system studied the transport time through the buffer is small compared with other transport timescales. As a result the differences between the main and variant sets of calculations are small. Nevertheless, if it were found that the transport timescale in the buffer was significant for a deep repository system, it would be important to investigate the sensitivity of the calculated fluxes from the near field to the method used to represent these diffusive fluxes.

The associated transfer rate between compartment  $i$  and compartment  $j$  is  $\lambda^{ij}$  given by:

$$\lambda^{ij} = \frac{1}{\kappa^i \Omega^{ij}}, \quad (2.3)$$

where  $\kappa^i$  is the capacity of compartment  $i$  defined by:

$$\kappa^i = \theta^i R^i V^i, \quad (2.4)$$

where  $\theta^i$  is the compartment porosity,  $R^i$  is the retardation coefficient for the radionuclide in question and  $V^i$  is the compartment volume.

Quintessa's interpretation of the transport lengths  $d$ , areas  $A$  and volumes  $V$  used is given in Table 2.1.4. It should be noted that the 'vertical' and 'horizontal' directions referred to in this table do not necessarily correspond with the directions referred to in SKB documentation.

In SR 97 analytical expressions are used for the transfer resistances from the source term into the buffer. For the canister-hole resistance Equation 2 of Hedin (2002) report was used:

$$\Omega = \frac{d_{Hole}}{D A_{Hole}} \quad (2.5)$$

where  $d_{Hole}$  is the length of the hole.

The resistance for the buffer-hole interface is taken as:

$$\Omega = \frac{1}{D \sqrt{2\pi} A_{Hole}} \quad (2.6)$$

#### *Transfer Resistances to Geosphere*

The four release locations have different properties. The fracture zones (Q1 and Q3) have extra resistance because of the small size, while Q2 and Q4 just have a flow resistance.

The flow resistances are represented by:

$$\Omega = \frac{1}{A_q \sqrt{q}}, \quad (2.7)$$

where  $A_q$  is a lumped parameter with values 0.03, 0.1, 1 and  $1 \text{ m}^{2.5} \text{ y}^{0.5}$  for Q1-Q4. Here  $q$  is the near-field Darcy flux (taken to have a value of  $0.002 \text{ m y}^{-1}$ ).

For Q1 and Q3 additional resistances are added according to

$$\Omega = \frac{B}{D}, \quad (2.8)$$

where  $B$  is another lumped parameter with dimensions  $\text{m}^{-1}$ . For Q1 this has a value of  $0.9 \text{ m}^{-1}$  and for Q3  $0.333 \text{ m}^{-1}$ .

It should be noted in passing that the calculated fluxes from the near field to the geosphere are very sensitive to the representation of the transfer resistances at interfaces (equations 2.5-2.8). It was not within the scope of the present study to assess the appropriateness of the representations employed by SKB, but in any regulatory review of a safety case that employed such models this would be an important consideration.

**Table 2.1.4.** Transport Lengths and Areas used in Resistances.

Compartment	d (m) (vertical transport)	A (m <sup>2</sup> ) (vertical transport)	d (m) (horiz. transport)	A (m <sup>2</sup> ) (horiz. transport)	Volume (m <sup>3</sup> )	Comment
B1	-	-	-	-	1.0	-
B2	-	-	0.05	variable	d A (horiz.)	Can thickness and hole area
B3.1	0.5	0.203	0.058	1.741	d A (vert.) 0.1016	Geometric values. The horizontal (radial) area is the area in the centre of the compartment.  The horizontal (radial) lengths are 1/6 of 35 cm (the buffer thickness).
B3.2	0.5	0.224	0.058	1.924	d A (vert.) 0.1122	
B3.3	0.5	0.246	0.058	2.107	d A (vert.) 0.1229	
B3.4	0.5	0.267	0.058	2.291	d A (vert.) 0.1336	
B3.5	0.5	0.289	0.058	2.474	d A (vert.) 0.1443	
B3.6	0.5	0.310	0.058	2.657	d A (vert.) 0.1550	
B4.1	1.0	2.405	-	-	d A (vert.) 2.4053	The area is the full cross sectional area of the deposition hole.
B4.2	3.33	2.405	-	-	d A (vert.) 8.0096	The height is to give the total can length of 4.833 m.
B5.1	0.5	2.405	-	-	d A (vert.) 1.2026	3 equal layers
B5.2	0.5	2.405	-	-	d A (vert.) 1.2026	
B5.3	0.5	2.405	-	-	d A (vert.) 1.2026	
B6	1.0	2.405	1.75	5.5	d A (vert.) 2.4053	1.75 m is the deposition hole diameter. 5.5 m is its circumference (times the 1 m height).

Compartment	d (m) (vertical transport)	A (m <sup>2</sup> ) (vertical transport)	d (m) (horiz. transport)	A (m <sup>2</sup> ) (horiz. transport)	Volume (m <sup>3</sup> )	Comment
B7.1	2.0	26.4	2.125	12.24	d A (horiz.) 26.010	2.125 m arises from a can separation of 6 m with 1.75 m for the deposition hole – half way to the next can. 12.24 m is probably the tunnel cross sectional area (e.g, Figures. 5-6 of the main SR 97 report, show a maximum height of 4 m and a maximum width of 3.6 m – with a rounded roof.)
B7.2	2.0	21.7	1.75	12.25	d A (horiz) 21.438	
B7.3	2.0	26.4	2.125	12.24	d A (horiz.) 26.010	
B8	0.5	2.405	-	-	d A (vert.) 1.2026	
B9	3.0	2.405	-	-	d A (vert.) 7.2158	The fracture zone is presumably 3 m below the deposition hole.

### 2.1.2 Intercomparisons

Figure 2.1.2 shows the fluxes from the near field for the chosen radionuclides for both the AMBER and Ecolego calculations. These figures show excellent agreement with the SKB calculations given in Figure 4.8 of Lindgren and Lindström (1999).

Table 2.1.5 gives details of the AMBER and Ecolego calculations. The SKB calculated peak fluxes for the three radionuclides with the highest peaks are also given in the table, and other information obtained directly from the SKB figure is given to one significant figure.

For peak radionuclide fluxes, the agreement between AMBER and the Ecolego calculations (and between these calculations and those given by SKB, where available) is to one significant figure or better. This is perfectly adequate for PA calculations. Detailed comparisons between the AMBER and Ecolego calculations revealed small differences arising from slightly different interpretations of the SKB model and data. These differences included the volumes used for compartments B4.1 and B4.2, and the use of different accuracies for input data (e.g., effective diffusivities). These differences are typical of those that arise when different models are used to implement the same test case, especially where the specification of the test case is open to different interpretations.

**Table 2.1.5.** Near-Field Calculations (*AMBER calculations are in normal font; EcoLego calculations are in italic font; SKB calculations are in bold font*).

	Peak flux [Bq y <sup>-1</sup> ] and time at which it occurs [y]	Total flux at 1000 years (and individual fluxes Q1-Q4) [Bq y <sup>-1</sup> ]	Total amount in the near-field at 1000 y [Bq]	Total flux at 10 000 years (and individual fluxes Q1-Q4) [Bq y <sup>-1</sup> ]	Total amount in the near-field at 10 000 y [Bq]
C-14	2.9E5 [2.2E4] <i>3.2E5 [2.2E4]</i> <b>3.0E5</b>	6.5E3 [5.0E3, 1.5E3, 1.0E1, 2.5E-1] <i>7.3E3 [5.7E3, 1.6E3, 1.1E1, 2.4E-1]</i> <b>7E3</b>	2.1E7 <i>2.0E7</i>	7.0E3 [3.3E3, 2.5E3, 1.2E3, 1.1E1] <i>7.3E3 [3.4E3, 2.6E3, 1.3E3, 1.2E1]</i> <b>6E3</b>	6.1E7 <i>7.1E7</i>
Cl-36	1.2E3 [5.7E4] <i>1.3E3 [5.7E4]</i> <b>1E3</b>	7.2E-1 [7.2E-1, 1.2E-3, 7.1E-5, 3.7E-7] <i>7.4E-1 [7.4E-1, 1.1E-3, 7.1E-5, 3.5E-7]</i>	1.6E4 <i>1.6E4</i>	6.5E0 [3.7E0, 1.6E0, 1.1E0, 3.0E-3] <i>7.1E0 [4.2E0, 1.7E0, 1.2E0, 3.0E-3]</i>	1.9E5 <i>1.9E5</i>
Ni-59	2.7E6 [2.0E4] <i>2.8E6 [2.1E4]</i> <b>2.8E6</b>	1.6E3 [1.6E3, 8.3E-1, 2.9E-6, 1.7E-6] <i>1.7E3 [1.7E3, 8.3E-1, 3.0E-6, 1.6E-6]</i> <b>2E3</b>	4.0E8 <i>4.0E8</i>	9.7E3 [6.7E3, 3.0E3, 4.5E0, 8.0E-2] <i>1.1E4 [7.9E3, 3.3E3, 5.1E0, 7.8E-2]</i> <b>1E4</b>	5.0E9 <i>5.0E9</i>
Se-79	6.3E1 [1.0E6]* <i>6.3E1 [8.7E5]</i> <b>6E1</b>	3.6E-3 [3.5E-3, 1.5E-4, 4.2E-7, 1.3E-9] <i>3.5E-3 [3.4E-3, 9.5E-5, 2.4E-7, 7.0E-10]</i>	5.9E1 <i>4.9E1</i>	2.8E-2 [1.3E-2, 1.1E-2, 3.7E-3, 4.8E-6] <i>3.1E-2 [1.5E-2, 1.2E-2, 4.3E-3, 4.7E-6]</i>	6.9E2 <i>6.5E2</i>
I-129	4.9E3 [3.6E4 y] <i>5.2E3 [3.6E4 y]</i> <b>5E3</b>	5.1E0 [5.0E0, 1.2E-1, 8.4E-3, 2.1E-5] <i>5.3E0 [5.2E0, 1.1E-1, 8.7E-3, 2.0E-5]</i>	4.7E4 <i>4.6E4</i>	3.9E1 [1.8E1, 1.2E1, 9.3E0, 5.1E-2] <i>4.2E1 [1.9E1, 1.3E1, 1.0E0, 4.9E-2]</i> <b>4E1</b>	4.7E5 <i>4.3E5</i>

	Peak flux [Bq y <sup>-1</sup> ] and time at which it occurs [y]	Total flux at 1000 years (and individual fluxes Q1-Q4) [Bq y <sup>-1</sup> ]	Total amount in the near-field at 1000 y [Bq]	Total flux at 10 000 years (and individual fluxes Q1-Q4) [Bq y <sup>-1</sup> ]	Total amount in the near-field at 10 000 y [Bq]
Cs-135	3.8E4 [2.1E4]  4.0E4 [2.1E4]  <b>3.7E4</b>	2.1E1 [2.1E1, 1.0E-2, 1.3E-8, 5.1E-8]  2.2E1 [2.2E1, 1.1E-2, 1.4E-8, 4.9E-8]  <b>2E1</b>	2.9E6  2.8E6	1.3E2 [9.6E1, 3.3E1, 1.9E-2, 2.4E-3]  1.5E2 [1.1E2, 3.6E1, 2.1E-2, 2.2E-3]  <b>1E2</b>	4.0E7  3.8E7
Ra-226	1.8E4 [1.0E6]*  1.1E4 [6.1 E5]  <b>2E4</b>	3.3E-5 [3.3E-5, 1.2E-7, 6.3E-13, 5.0E-13]  2.4E-5 [2.3E-5, 5.5E-8, 2.3E-13, 1.9E-13]	1.2E0  7.3E-1	7.8E-2 [6.4E-2, 1.4E-2, 9.5E-6, 7.6E-7]  1.1E-1 [9.1 E-2, 1.9E-2, 1.3E-5, 9.2E-7]	5.1E3  6.2E3
Pu-239	6.3E1 [6.8E4]  1.3E2 [1.3E5]  <b>1E2</b>	1.1E-7 [1.1E-7, 4.0E-15, 0, 0]  1.7E-7 [1.7E-7, 6.0E-15, 0, 0]	5.2E3  7.7E3	4.0E-3 [3.9E-3, 1.6E-9, 0, 0]  5.9E-3 [5.9E-3, 2.3E-9, 0, 0]	6.7E4  9.5E4

\* still increasing at end of simulation period

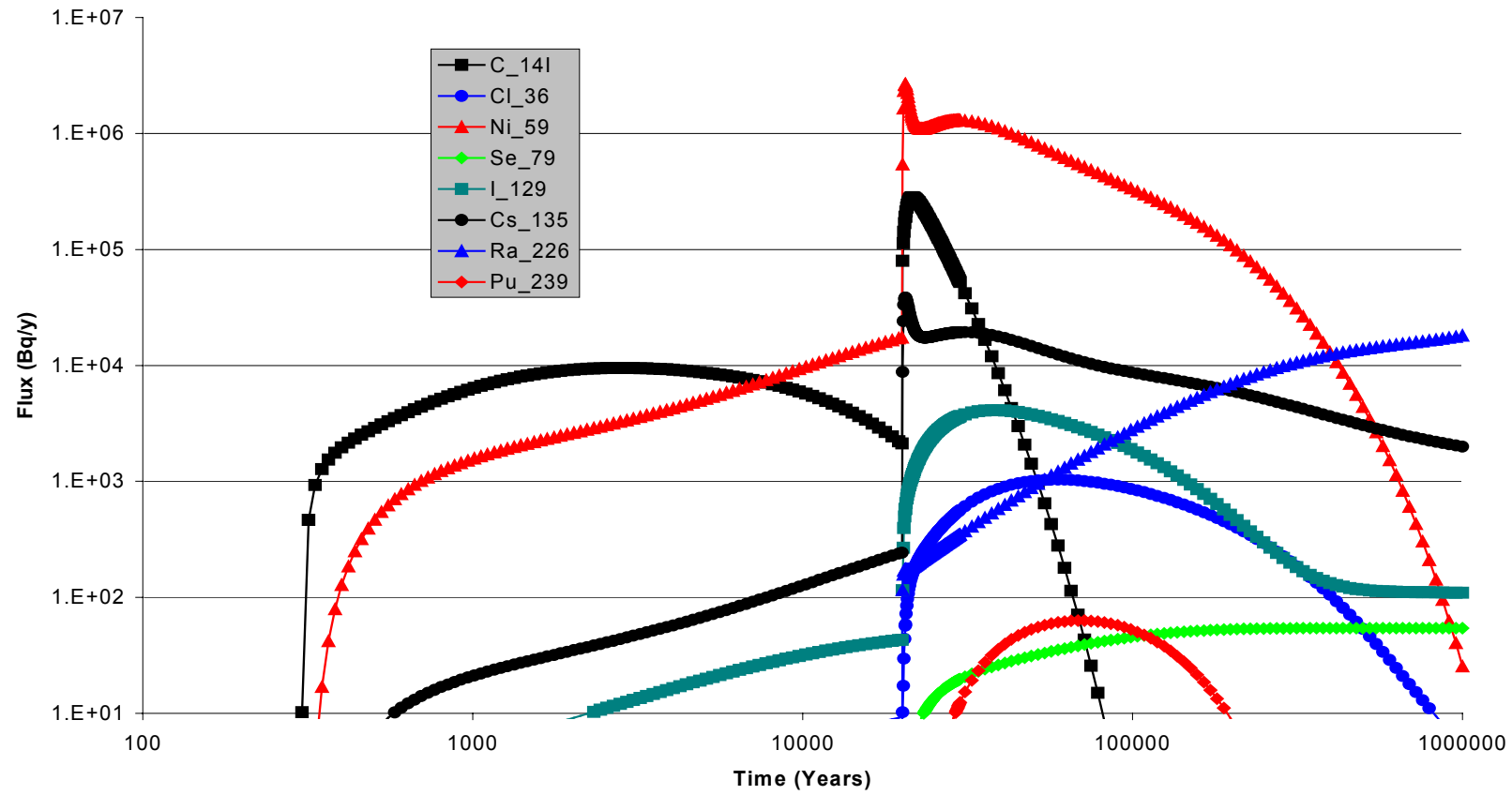


**Figure 2.1.2a** Fluxes from the Near Field for the AMBER Calculations.

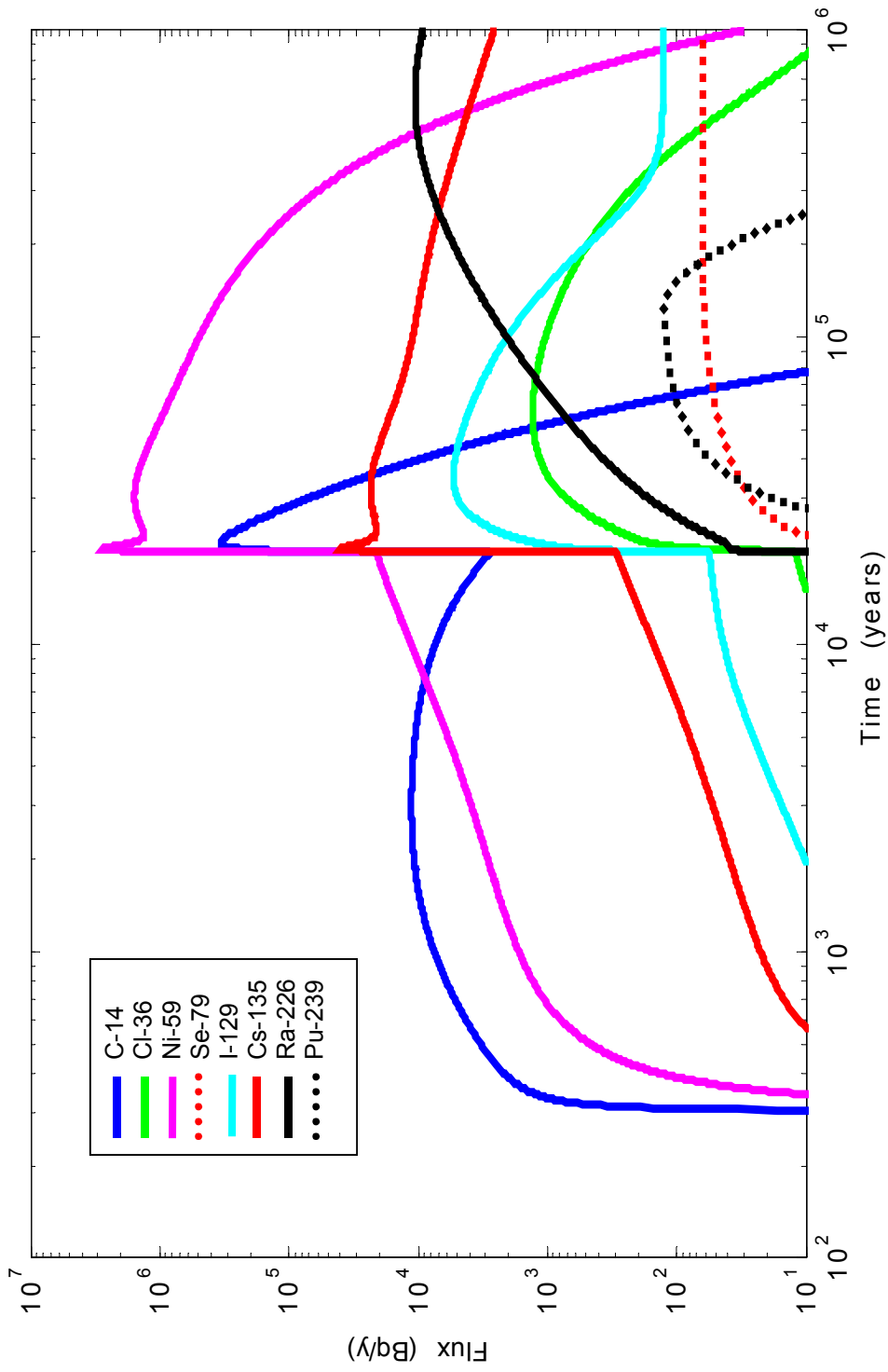


**Figure 2.1.2b** Fluxes from the Near Field for the Ecolego Calculations.

## 2.2 The Geosphere

### 2.2.1 Test Case Specification

In the far field the SR 97 calculations used FAR31 (Norman and Kjellbert, 1990). FAR31 is a one-dimensional advection-dispersion and matrix diffusion code comparable to CRYSTAL (Worgan and Robinson, 1995). Again, the model comparisons described in Section 4.2.1 in Lindgren and Lindström (1999) were used as the basis of the main intercomparison case. This calculation is for the Aberg site.

The information given in Lindgren and Lindström (1999) and Hedin (2002) is adequate to define all the parameters that need to be used. A summary of data sources is given in Table 2.2.1.

The AMBER calculations used a compartmental approach to geosphere modelling whilst the Ecolego calculations used an implementation of the algorithms similar to CRYSTAL.

One of the main aims of this part of the main test case was to compare the use of a semi-analytical method for the geosphere transport calculations (in CRYSTAL and Ecolego) with an approximation to this using a compartmental approach (in AMBER).

**Table 2.2.1.** Geosphere Data Sources.

Parameter	Data Source
Fracture half-width	1E-4 m. TR-99-23 Table 3-14 and Hedin Table V.
Flow wetted surface area per volume of water	1E4 m <sup>-1</sup> . 'Reasonable' Aberg value TR-99-23 Table 3-15. Consistent with specified fracture half-width.
Geosphere path length	500 m. Assumed value
Geosphere travel time	10 y. 'Reasonable' Aberg value TR-99-23 Table 3-15 and Hedin Table V.
Groundwater velocity in fracture	50 m y <sup>-1</sup> . Derived from path length and travel time
Matrix penetration depth	2 m. TR-99-23 Table 3-15 and Hedin Table V.
Fracture porosity	5E-5. Consistent with specified fracture half-width and matrix penetration depth.
Peclet number	10. 'Reasonable' Aberg value TR-99-23 Table 3-15 and Hedin Table V.
Longitudinal diffusivity in fracture	2500 m <sup>2</sup> y <sup>-1</sup> . Derived from Peclet number (10), groundwater velocity and path length
Rock porosity and density	0.005 and 2700 kg m <sup>-3</sup> . TR-99-23 Table 3-13 and Hedin Table V.
Matrix Effective Diffusivities (element-dependent)	TR-99-23 Table 3-12 and Hedin Table IV. Note that the pore water diffusivity is this value divided by the rock porosity.
Distribution coefficients for rock	'Reasonable' Aberg values TR-99-23 Table 3-11 and Hedin Table IV.
Retardation on fracture wall	1. Hedin Table V.
Outlet boundary condition	Zero concentration

### 2.2.2 The Representation of the Geosphere in AMBER

For compartment models the minimum number  $N$  of components to be used in the direction of radionuclide transport can be determined by the Peclet number  $Pe$ . If  $N$  is chosen so that

$$N = \frac{Pe}{2}, \quad (2.9)$$

then the numerical dispersion introduced will be equivalent to that anticipated by dispersion.

The AMBER far field sub-model therefore discretises the flowing fracture into 5 compartments, consistent with a Peclet number in the region of 10. A relatively large number of rock matrix compartments is needed when calculations are undertaken for a number of different radionuclides with different sorption coefficients; for calculations with a single radionuclide a smaller number of compartments is adequate. Six compartments are used with the sizes of the matrix compartments increasing by a specified factor from the fracture to the diffusion limit. It is found that a factor of 3 generally gives good results.

It is assumed that the walls of the fracture compartments (to a depth  $\delta$ ) are in equilibrium with flowing water. This introduces an effective fracture retardation coefficient  $R_f$  given by

$$R_f = 1 + \frac{2\delta(\theta + \rho K_d)}{a}, \quad (2.10)$$

where  $\theta$  is the rock porosity (unitless),  $\rho$  is its density ( $\text{kg m}^{-3}$ ),  $a$  is the fracture half-aperture (m) and  $K_d$  is the relevant equilibrium sorption coefficient ( $\text{m}^3 \text{kg}^{-1}$ ). This is effectively the same as introducing a very thin first rock matrix compartment, and can be important for strongly sorbed radionuclides.

An appropriate value for the equilibrium layer thickness on the fracture wall can be obtained by equating a timescale for radionuclide mixing across this thickness of rock with the timescale for transport along the fracture. One then has:

$$\frac{\delta^2 R}{2D} = \tau_g R_f, \quad (2.11)$$

where  $R$  is the retardation factor in the rock,  $D$  is the effective diffusivity in the rock and  $\tau_g$  is the geosphere travel time for an unsorbed radionuclide. Using the parameter values employed in this calculation gives a value of  $\delta$  for strongly sorbed radionuclides of  $2 \times 10^{-3}$  m.

In summary, the approach that has been taken to the discretisation of the rock matrix is to employ compartments with geometrically increasing thickness away from the fracture

with equilibrium conditions assumed in a thin layer in contact with the fracture. A suitable factor for the ratio of neighbouring compartment sizes has been found to be 3.

Figure 2.2.1 gives a comparison between the geosphere response functions (the flux for a unit input at time  $t=0$ ) calculated by AMBER and those calculated by CRYSTAL. The shapes of the AMBER response functions show clearly that with a compartmental approach to matrix diffusion it is possible to reproduce the calculations of semi-analytical models fairly closely (adequate for PA calculations) if a suitable choice is made for the matrix compartment dimensions. The response function shapes will, however, always give an indication of the approximations that have been made. Effectively, the compartment model calculations represent a fit to the actual response function using a number of exponential functions. The very early differences in the response function for Cl-36 in Figure 2.2.1 are due to the different treatment of longitudinal dispersion in the fracture; closer agreement could be obtained by using more compartments in the direction of groundwater flow, but the differences are generally not important for the calculation of radiological impacts.

### 2.2.3 The Representation of the Geosphere in Ecolego

Transport of radionuclides in fractured rocks can be described by a 1-D advection-dispersion equation for the fracture and a 1-D diffusion/sorption equation for the porous matrix coupled by the continuity of concentration along the interface (e.g. Sudicky and Frind, 1982; Hodgkinson and Maul, 1988; Xu and Wörman, 1999 and Hedin, 2002):

$$\frac{\partial C_n}{\partial t} + u \frac{\partial C_n}{\partial x} - D \frac{\partial^2 C_n}{\partial x^2} + \lambda_n C_n - \lambda_{n-1} C_{n-1} - \frac{D_e}{b} \frac{\partial C_n^p}{\partial z} \Big|_{z=0} = 0 \quad (2.12)$$

$$R_n^p \frac{\partial C_n^p}{\partial t} - D_e \frac{\partial^2 C_n^p}{\partial z^2} + R_n^p \lambda_n C_n^p - R_{n-1}^p \lambda_{n-1} C_{n-1}^p = 0 \quad (2.13)$$

With the retardation factors due to sorption into the rock matrix defined by

$$R_n^p = \theta_p + (1 - \theta_p) K_{d,n} \rho \quad (2.14)$$

where

$C_n$  = concentration of radionuclide n in the fracture water [moles  $\text{m}^{-3}$ ]

$C_n^p$  = concentration of radionuclide n in the matrix water [moles  $\text{m}^{-3}$ ]

$u$  = groundwater velocity [ $\text{m y}^{-1}$ ]

$D$  = dispersion coefficient [ $\text{m}^2 \text{y}^{-1}$ ]

$b$  = half width of fracture [m]

$x$  = distance along fracture [m]

$z$  = distance into matrix orthogonal to fracture surface [m]

$D_e$  = effective matrix diffusivity [ $\text{m}^2 \text{y}^{-1}$ ]

$K_{d,n}$  = distribution coefficient for radionuclide n inside rock matrix [ $\text{m}^3 \text{kg}^{-1}$ ]

$\theta_p$  = matrix porosity [-]

$\lambda_n$  = decay constant for radionuclide n [ $\text{y}^{-1}$ ]

$\rho$  = bulk density of rock matrix [ $\text{kg m}^{-3}$ ]

For a solute pulse travelling in the fracture (a delta source), the initial and boundary conditions are:

$$C_n(x, t = 0) = C_n^p(x, t = 0) = 0 \quad (2.15)$$

$$C_n(x = 0, t) = \delta(t) \frac{M_0}{Q} \quad (2.16)$$

$$C_n^p(z = 0, t) = C_n(x, t) \quad (2.17)$$

$$\left. \frac{\partial C_n^p}{\partial z} \right|_{z=L} = 0 \quad (2.18)$$

$$C_n(x, t = \infty) = 0 \quad (2.19)$$

in which  $Q$  is the water flux [ $\text{m}^3 \text{y}^{-1}$ ],  $M_0$  is the total mass of solute inserted into the fracture [moles],  $\delta(t)$  is the Dirac delta function [ $\text{y}^{-1}$ ] and  $L$  is the maximum diffusion depth [m].

A solution to equations (2.12) and (2.13) with the initial and boundary conditions (2.14) to (2.19) can be obtained by eliminating the time derivative and introducing a Laplace transform variable  $p$ . The transformed equations are following:

$$\bar{C}_n(p + \lambda_n) + u \frac{\partial \bar{C}_n}{\partial x} - D \frac{\partial^2 \bar{C}_n}{\partial x^2} - \lambda_{n-1} \bar{C}_{n-1} - \frac{D_e}{b} \left. \frac{\partial \bar{C}_n^p}{\partial z} \right|_{z=0} = 0 \quad (2.20)$$

$$R_n^p(p + \lambda_n) \bar{C}_n^p - D_e \frac{\partial^2 \bar{C}_n^p}{\partial z^2} - R_{n-1}^p \lambda_{n-1} \bar{C}_{n-1}^p = 0 \quad (2.21)$$

$$\bar{C}_n(x = 0, p) = \frac{M_0}{Q} \quad (2.22)$$

$$\bar{C}_n^p(z = 0, p) = \bar{C}_n(x, p) \quad (2.23)$$

$$\left. \frac{\partial \bar{C}_n^p}{\partial z} \right|_{z=L} = 0 \quad (2.24)$$

Similar to those of Hodgkinson and Maul (1988), the general descriptions of radionuclide concentrations in pore water can be expressed as

$$\bar{C}_n^p(x, z, p) = \sum_{m=1, n} \bar{C}_m(x, p) y_{mn}(z, p) \quad (2.25)$$

$$y_{mn}(z, p) = \frac{\cosh[\alpha_n(p)(L - z)]}{\cosh[\alpha_n(p)L]} \quad (2.26)$$

$$y_{mn}(z, p) = \left( \prod_{k=m, n-1} \frac{R_k^p \lambda_k}{D_{e, k+1}} \right) \sum_{k=m, n} \frac{y_{kk}(z, p)}{\prod_{\substack{l=m, n \\ l \neq k}} [\alpha_l^2(p) - \alpha_k^2(p)]} \quad (2.27)$$

where

$$\alpha_n = \sqrt{\frac{(p + \lambda_n) R_n^p}{D_{e, n}}} \quad (2.28)$$

Substituting the derivative of the pore water concentration at  $z=0$  into (2.20), a solution for the concentration in the fracture can be derived straightforwardly with the initial and boundary conditions. The inversion of the solution to the real time domain cannot be obtained analytically. Instead, a solution is obtained with a numerical inversion code (Hollenbeck, 1998) based on the series expansion method of De Hoog et al. (1982). Finally the output from geosphere is obtained by convolution with the near field release. The numerical solver for the far field has been implemented as a “build-in” function in Ecolego.

#### 2.2.4 Intercomparisons

Figure 2.2.2 give the fluxes from the geosphere calculated using AMBER and Ecolego with the input flux from the near field. These figures show excellent agreement with the SKB calculations given in Figure 4.8 of Lindgren and Lindström (1999).

Table 2.2.2 gives detailed AMBER/Ecolego comparisons. As before, the SKB calculated peak fluxes for the three radionuclides with the highest peaks are also given in the table to two significant figures, and other information obtained directly from the SKB figure is given to one significant figure. The main observations that can be made from these comparisons are:

- The closeness of the AMBER calculations for the geosphere response function (with unit input) to the Ecolego calculations is similar to that for the CRYSTAL calculations (Section 2.2.1) as expected. Because AMBER used an approximate solution to the equations for matrix diffusion, exact agreement between the two sets of calculations cannot be obtained. With the matrix discretisation employed, the AMBER calculations appear to slightly overestimate the peak flux associated with a slightly earlier peak time.
- For peak radionuclide fluxes from the geosphere, the agreement between the AMBER and Ecolego calculations (and between these calculations and those given by SKB, where available) is generally one significant figure. This is perfectly adequate for PA calculations. This does not apply to Pu-239 where the fluxes are very low throughout the simulation period; the compartmental approach for the geosphere in AMBER does not give a good approximation to the radionuclide flux in this situation.

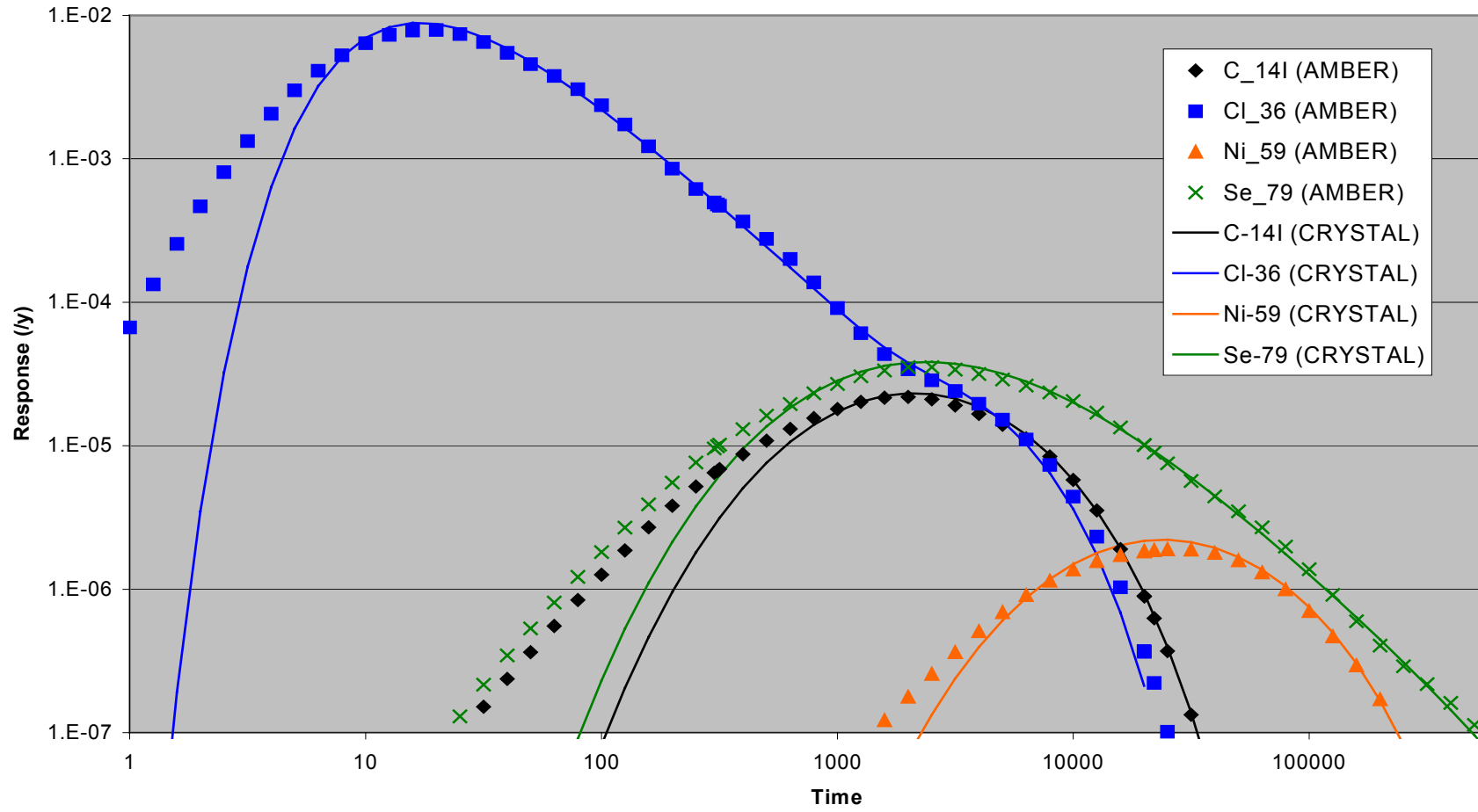


**Figure 2.2.1.** Geosphere Response Functions for AMBER and CRYSTAL.

**Table 2.2.2.** Geosphere Calculations (AMBER calculations are in normal font; Ecolego calculations are in *italic* font; SKB calculations are in **bold** font).

Radionuclide	Peak Flux for unit input at t=0 [Bq y <sup>-1</sup> ] and time at which it occurs [y]	Peak Flux [Bq y <sup>-1</sup> ] for the calculated near-field flux and time at which it occurs [y]	Flux at 10 000 years [Bq y <sup>-1</sup> ]	Flux at 100 000 years [Bq y <sup>-1</sup> ]
C-14	2.2E-5 [1.9E3] <i>1.8E-5 [2.3E3]</i>	2.3E4 [2.7E4] <i>2.3E4 [2.7E4]</i> <b>2.1E4</b>	1.1E3 <i>1.1E3</i> <b>1E3</b>	1.6E0 <i>1.3E0</i>
Cl-36	8.0E-3 [1.8E1] <i>7.4E-3 [1.9E1]</i>	1.2E3 [5.9E4] <i>1.3E3 [5.8E4]</i> <b>1E3</b>	5.9E0 <i>6.3E0</i>	9.9E2 <i>1.1E3</i> <b>1E3</b>
Ni-59	1.9E-6 [2.8E4] <i>1.8E-6 [2.7E4]</i>	9.3E4 [9.1E4] <i>1.0E5 [9.9E4]</i> <b>9.9E4</b>	2.3E1 <i>1.5E1</i> <b>1E1</b>	9.2E4 <i>1.0E5</i> <b>1E5</b>
Se-79	3.6E-5 [2.3E3] <i>3.2E-5 [2.7E3]</i>	5.4E1 [1.0E6] <i>4.2E1 [4.1E5]</i> <b>5E1</b>	4.3E-3 <i>4.4E-3</i>	3.6E1 <i>1.5E1</i> <b>3E1</b>
I-129	8.0E-3 [1.8E1] <i>7.4E-3 [1.9E1]</i>	4.8E3 [3.7E4] <i>5.3E3 [3.7E4]</i> <b>5.0E3</b>	3.6E1 <i>4.0E1</i> <b>4E1</b>	2.1E3 <i>2.1E3</i> <b>2E3</b>
Cs-135	3.2E-7 [2.5E5]	1.2E3 [9.1E5]	4.6E-3	1.7E2

Radionuclide	Peak Flux for unit input at t=0 [Bq y <sup>-1</sup> ] and time at which it occurs [y]	Peak Flux [Bq y <sup>-1</sup> ] for the calculated near-field flux and time at which it occurs [y]	Flux at 10 000 years [Bq y <sup>-1</sup> ]	Flux at 100 000 years [Bq y <sup>-1</sup> ]
	<i>2.7E-7 [2.6E5]</i>	<i>1.1E3 [8.7E5]</i> <b>1E3</b>	<i>6.0E-5</i>	<i>1.0E2</i> <b>1E2</b>
Ra-226	5.8E-8 [3.5E3] <i>2.4E-8 [5.3E3]</i>	7.2E0 [1.0E6]* <i>1.2E1 [1.0E6]*</i>	7.1E-6 <i>2.2E-6</i>	1.0E0 <i>8.9E-1</i>
Pu-239	1.5E-12 [8.6E4] <i>1.4E-15 [2.0E5]</i>	4.4E-6 [1.9E5] <i>2.0E-8 [3.3E5]</i>	8.9E-16 <i>8.4E-29</i>	1.0E-6 <i>1.6E-11</i>

\* still increasing at end of simulation period

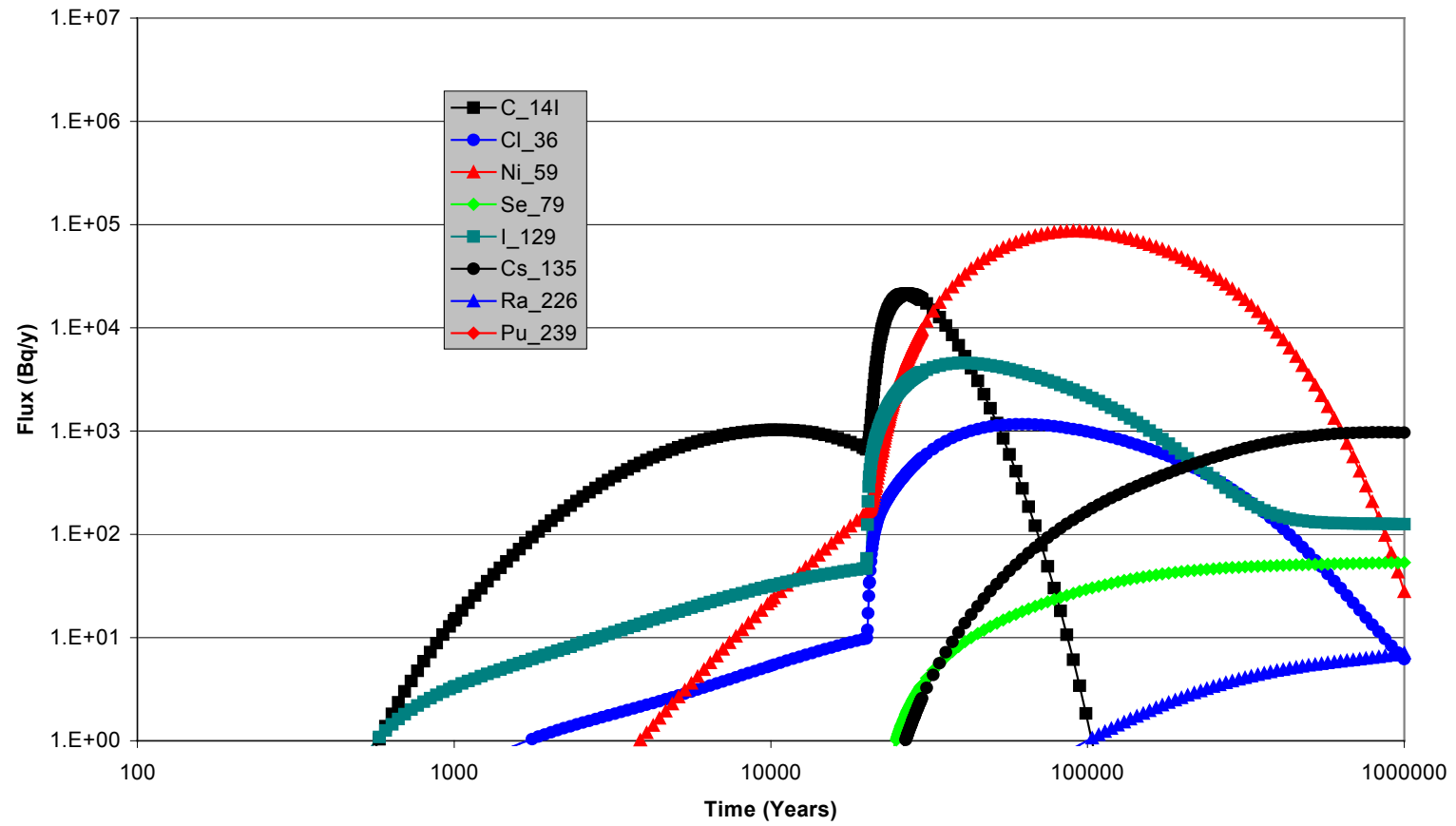


**Figure 2.2.2a.** Fluxes from the Geosphere with the Near-Field Source Calculated by AMBER.

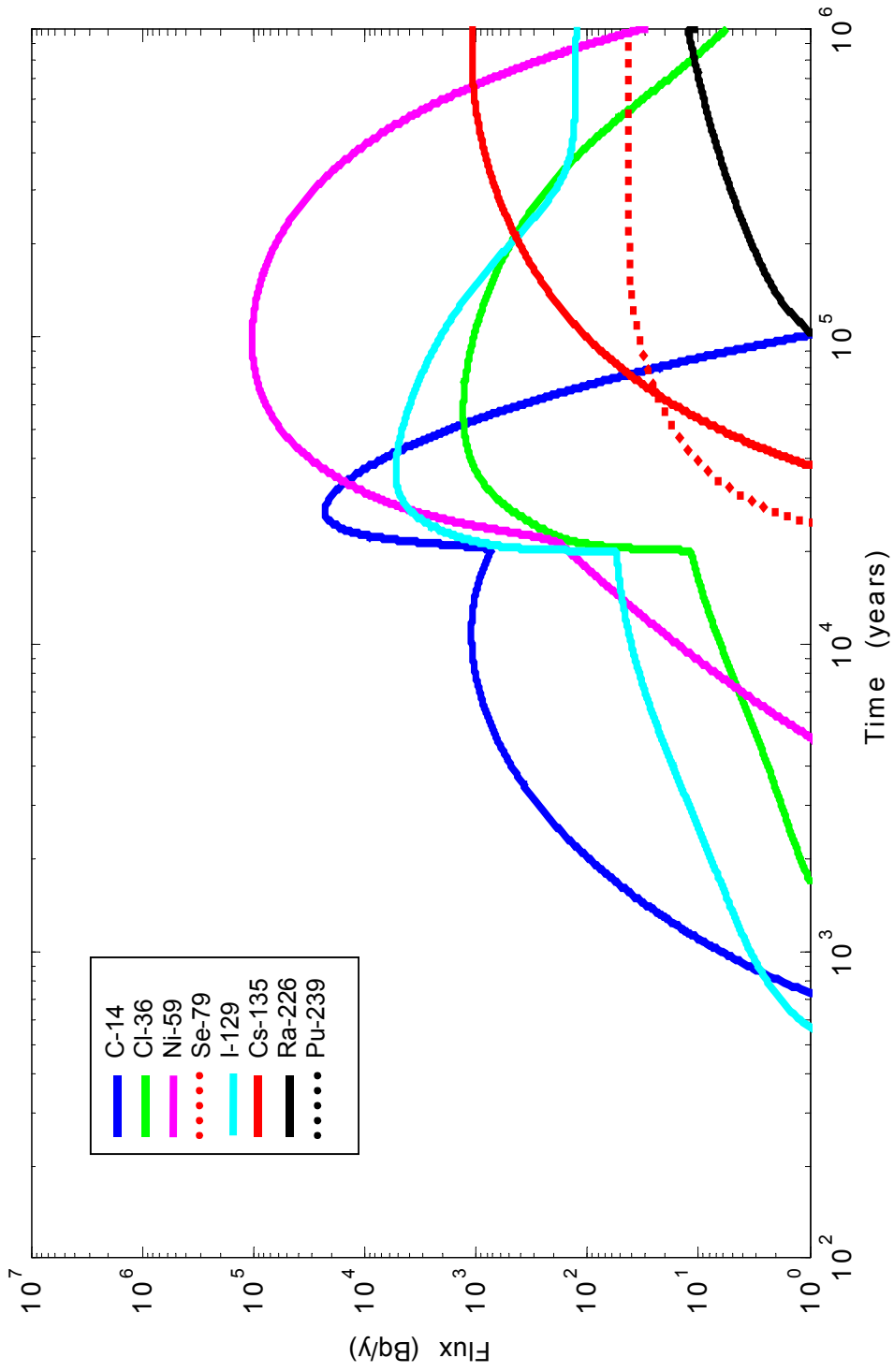


**Figure 2.2.2b** Fluxes from the Geosphere with the Near-Field Source Calculated by Ecolego.

## 2.3 The Biosphere

### 2.3.1 Test Case Specification

#### Model Structure and Radionuclide Transport

The coastal biosphere described by Bergström et al. (1999) provides the basis for this test case. It should be noted that this is not the biosphere considered in Section 4.2.1 of Lindgren and Lindström (1999); a more complicated Peat Bog system was used there. The compartment structure of the coastal model is shown in Figure 2.3.1. In the description of the model given by Bergström et al. (1999) the suspended sediment compartments are not included, although they are included in the Norlinder et al. (1997) reference given in that report. Calculations with this model indicated that the suspended sediment compartments needed to be included in order to obtain reasonable agreement with the calculations reported by SKB. It would therefore appear that the description of the biosphere model in Bergström et al. (1999) does not correspond exactly with the reported SKB calculations.

For this deterministic case, best estimate values have been used for all parameters. Simple transfer rates are specified for exchanges between water bodies and the following equations are used to determine transfers involving sediment compartments.

From the description of the model in Norlinder et al. (1997), the transfer rate from the water phase to suspended sediment is given by (in the current notation):

$$\lambda_{wss} = \frac{K_d \ln 2 S}{\tau \rho_w} \quad (2.29)$$

where  $K_d$  is the sorption coefficient onto suspended sediment ( $\text{m}^3 \text{kg}^{-1}$ ),  $S$  is the suspended sediment load ( $\text{kg m}^{-3}$ ),  $\rho_w$  is the density of water ( $1000 \text{ kg m}^{-3}$ ) and  $\tau$  is the parameter described as the 'half-time of the reaction velocity', taken to be 1 month (0.083 years).

However, this is dimensionally incorrect, and it is assumed that the actual expression employed may have been:

$$\lambda_{wss} = \frac{(\rho_s K_d) \ln 2 S}{\tau \rho_w} \quad (2.30)$$

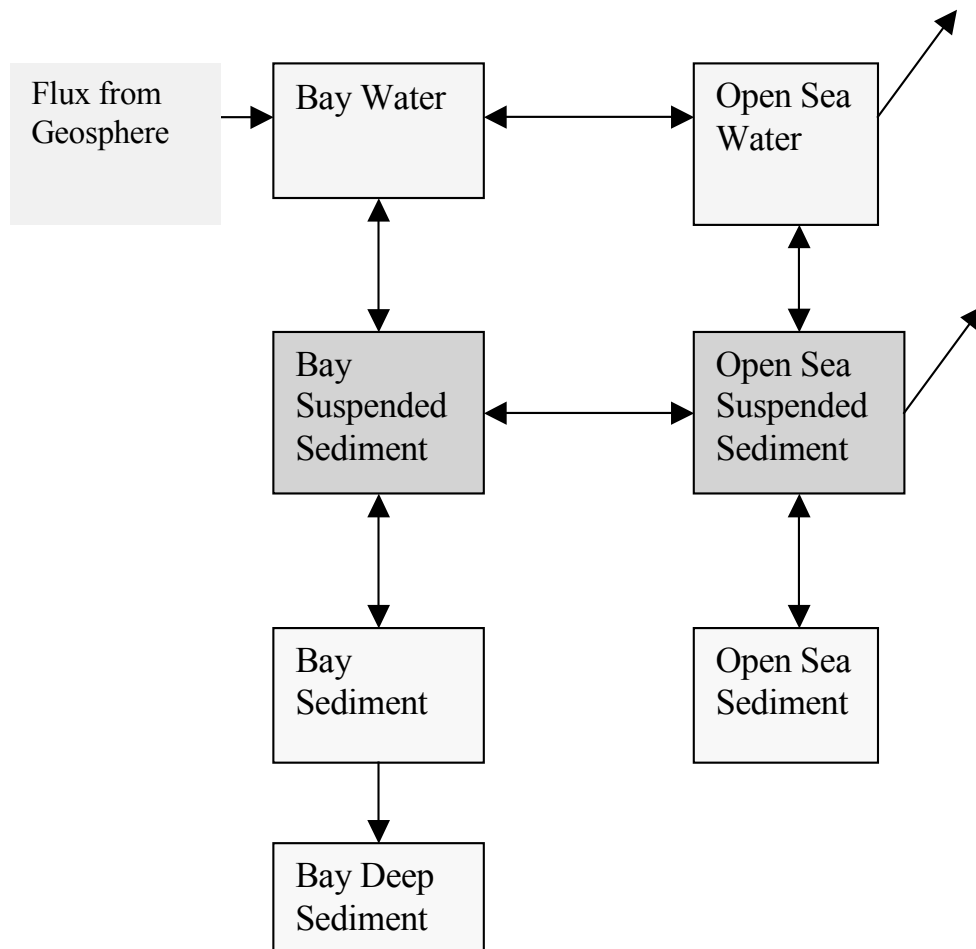


**Figure 2.3.1.** Biosphere Compartment Structure.

where  $\rho_s$  is the density of sediments (taken to be  $1600 \text{ kg m}^{-3}$ ). This expression has therefore been used in the calculations employed below, although it is considered that the correct expression to use would not include the densities of water and sediment. This uncertainty about the exact expression that was used by SKB for the transfer of radionuclides from solution to sediment does not lead to significant uncertainties in the calculations.

The transfer rate in the opposite direction from suspended sediment to the water phase is given by:

$$\lambda_{ssw} = \frac{\ln 2}{\tau} \quad (2.31)$$

For radionuclide transport from the suspended sediment phase to bottom sediments one has:

$$\lambda_{ws} = \frac{\sigma}{Sd}, \quad (2.32)$$

where  $\sigma$  is the gross sedimentation rate ( $\text{kg m}^{-2} \text{ y}^{-1}$ ) and  $d$  is the depth of the water compartment (m).

Transport in the opposite direction due to resuspension in the Bay is given by:

$$\lambda_{sw} = \exp\left(-\frac{1000 k d_m}{\sqrt{A}}\right), \quad (2.33)$$

where  $d_m$  is the maximum depth of the water body (m),  $k$  is an empirical factor and  $A$  is its area ( $\text{m}^2$ ). It should be noted that the dimensions of this expression are incorrect (the transfer rate should have units of  $1/\text{time}$ , but is dimensionless). Units of  $\text{y}^{-1}$  have been assumed for this parameter (this appears to be what has been done in Bergström et al. (1999)). A constant value for this resuspension transfer is used for the Open Sea.

Transport from upper to deep sediments in the Bay is represented by:

$$\lambda_{sd} = \frac{\sigma}{\mu} - \lambda_{sw}, \quad (2.34)$$

where  $\mu$  is the mass of upper sediment per unit area ( $\text{kg m}^{-2}$ )

### **Radionuclide Concentrations in Foods and Critical Group Doses**

The exposure pathways considered are consumption of sea fish, algae, milk and meat. In each case the critical group dose rate for a given radionuclide is calculated from

$$H = \kappa \alpha \chi_F, \quad (2.35)$$

where, in consistent units,  $H$  is the dose rate ( $\text{Sv y}^{-1}$ ),  $\kappa$  is the dose rate for unit activity ingested ( $\text{Sv Bq}^{-1}$ ),  $\alpha$  is the consumption rate ( $\text{kg y}^{-1}$ ) and  $\chi_F$  is the concentration in the relevant food ( $\text{Bq/kg}$ ).

For the sea fish and algae pathways the concentration in food is given simply by

$$\chi_F = F \left( C_w + \frac{\chi_s}{\rho_w} \right), \quad (2.36)$$

where  $F$  is the relevant concentration factor ( $\text{m}^3 \text{kg}^{-1}$ ) and  $C_w$  ( $\text{Bq m}^{-3}$ ) and  $\chi_s$  ( $\text{Bq kg}^{-1}$ ) are the radionuclide concentrations of in the relevant compartments. Two points arise from the way that these algorithms appear to have been applied by SKB:

- The concentration factors relate to the amount of radioactivity in unit volume of water, including the suspended sediment.
- The sea fish is assumed to be harvested from the Bay compartment but the algae is assumed to be harvested from the Open Sea compartment (this is not stated explicitly in the relevant section of Bergström et al. (1999)).

For meat and milk consumption the concentration in food is given by:

$$\chi_F = IT, \quad (2.37)$$

where  $I$  ( $\text{Bq y}^{-1}$ ) is the intake rate of radionuclides and  $T$  is the relevant transfer factor ( $\text{y kg}^{-1}$ ). The radionuclide intake of the cattle is assumed to be due to drinking water from the Bay and consuming water plants (this is not totally clear in the SKB documentation):

$$I = f \left\{ \alpha_w \left( C_w + \frac{\chi_s}{\rho_w} \right) + \alpha_p \chi_p \right\}, \quad (2.38)$$

where  $f$  is the fraction of the time spent grazing on the shoreline,  $\alpha_w$  is the cattle's consumption rate of water ( $\text{m}^3 \text{y}^{-1}$ ),  $\alpha_p$  is the cattle's consumption rate of water plants ( $\text{kg y}^{-1}$ ) and  $\chi_p$  is the radionuclide concentration in water plants ( $\text{Bq kg}^{-1}$ ) which appears to have been derived from:

$$\chi_p = \frac{(C_w + \frac{\chi_s}{\rho_w}) T_r \tau}{\rho_w Y}, \quad (2.39)$$

where, in consistent units,  $T_r$  is the transpiration rate ( $\text{kg m}^{-2} \text{y}^{-1}$ ),  $\tau$  is the mean time for transpiration before the water plant is eaten by the cattle ( $\text{y}$ ) and  $Y$  is the yield of the water plants ( $\text{kg m}^{-2}$ ).

It should be noted that the description of the algorithms used to calculate radionuclide concentrations in foods is not totally clear in Bergström et al. (1999), so it is possible

that there could be some differences between the implementation of these algorithms in AMBER/Ecolego and SKB.

A summary of the data sources that have been used is given in Table 2.3.1.

### *2.3.2 Intercomparisons*

Table 2.3.2 gives details of the AMBER and Ecolego calculations. It should be noted that the equilibrium dose rates for a unit flux of radioactivity from the geosphere are close to, but not identical to, the mean values presented in Table 4-10 of Bergström et al. (1999) from a probabilistic calculation (see Section 3).

The main observations that can be made from these comparisons are:

- The essentially identical calculations for the equilibrium inventories in Bay sediments illustrates that the calculations by AMBER and Ecolego of radionuclide transport around the biosphere system are the same.
- Small differences in the calculated equilibrium dose rates for unit input to the biosphere system are believed to be due to residual differences in the way that the algorithms for the calculation of radionuclide concentrations in environmental materials and resulting exposures. This may be due to differences in the interpretation of the SKB documentation in this area.

**Table 2.3.1.** Biosphere Data Sources.

Parameter	Data Source
Human consumption rates $\alpha$ for algae, drinking water, meat milk and sea fish	TR-99-14 Table B-2
Dimensions of Bay and Opens Sea (area $A$ , depth $d$ and volume)	TR-99-14 Table 3-11
Water exchange rates between aquatic compartments	TR-99-14 Table 3-11
Sediment parameters (gross sedimentation rate $\sigma$ , suspended sediment loads $S$ , mass of top sediment per units area $\mu$ and resuspension rate for Open Sea sediments)	TR-99-14 Table 3-12
Bulk density of sediments	1600 kg m <sup>-3</sup>
Sediment sorption coefficients, $K_d$	TR-99-14 Table A-9
Concentration factors for algae, $F$	TR-99-14 Table A-14
Concentration factors for sea fish, $F$	TR-99-14 Table A-13
Cattle consumption rates of water and algae, $\alpha$	TR-99-14 Table B-1
Time spent by cattle grazing by the shore $f$	TR-99-14 Table B-1
Plant transpiration time $\tau$	TR-99-14 Table B-1
Transfer coefficients to milk $T$	TR-99-14 Table A-10
Transfer coefficients to meat $T$	TR-99-14 Table A-11
Water plant transpiration rate $T_r$	TR-99-14 Table 3-12
Yield of water plants $Y$	TR-99-14 Table 3-12

**Table 2.3.2.** Biosphere Calculations (*AMBER calculations are in normal font. Ecolego calculations are in italic font*).

Radionuclide	Equilibrium Dose rate to Critical Group for a unit input flux of 1 Bq/y from the geosphere [Sv/y]	Peak Dose rate to Critical Group for the calculated flux from the geosphere [Sv/y]	Equilibrium amount in Bay sediments for a unit input flux of 1 Bq/y from the geosphere [Bq]
C-14	1.4E-15 <i>1.4E-15</i>	3.0E-11 <i>3.2E-11</i>	8.1E-6 <i>8.1E-6</i>
Cl-36	1.2E-16 <i>9.9E-17</i>	1.5E-13 <i>1.3E-13</i>	8.1E-6 <i>8.1E-6</i>
Ni-59	2.9E-17 <i>2.8E-17</i>	2.6E-12 <i>2.9E-12</i>	8.0E-2 <i>8.0E-2</i>
Se-79	1.3E-14 <i>1.3E-14</i>	7.1E-13 <i>5.7E-13</i>	4.0E-2 <i>4.0E-2</i>
I-129	1.9E-14 <i>1.5E-14</i>	8.8E-11 <i>7.7E-11</i>	2.4E-3 <i>2.4E-3</i>
Cs-135	7.3E-16 <i>6.5E-16</i>	7.2E-13 <i>7.1E-13</i>	8.0E-2 <i>8.0E-2</i>
Ra-226	1.8E-14 <i>1.8E-14</i>	1.3E-13 <i>2.2E-13</i>	7.9E-2 <i>7.9E-2</i>
Pu-239	7.5E-15 <i>7.5E-15</i>	3.2E-20 <i>1.5E-22</i>	7.0E-1 <i>7.0E-1</i>

## 2.4 Sensitivity Calculations

It can be argued that the representation of the growth of the canister hole in the SKB calculations is somewhat arbitrary. Although outside the scope of the AMBER/Ecolego intercomparison study, some sensitivity calculations were undertaken to investigate the potential importance of the parameter choices made; Table 2.4.1 gives the details.

**Table 2.4.1:** Sampled Parameters in Sensitivity Calculations.

Parameter	SR 97 Value	Probability Density Function
Initial Hole Size	1E-6 m <sup>2</sup>	Log uniform, 1E-8 to 1E-4 m <sup>2</sup>
Final Hole Size	1E-2 m <sup>2</sup>	Log uniform, 1E-3 to 1E-1 m <sup>2</sup>
Time when final hole size reaches final value	20 000 y	Uniform, 1E4 to 1E5 y

For the range of parameters considered, by far the most important parameter is the final size of the hole; its initial size and the time taken to reach the final size are much less important. Figure 2.4.1 gives a scatter plot produced by AMBER that indicates how the calculated peak annual dose (summed over the radionuclides considered) varies for this parameter; there is a strong correlation between the calculated peak dose and the final hole size, with around an overall order of magnitude variation in the annual dose.

It should be emphasised that it is not suggested that the parameter ranges chosen are realistic; they were simply used to investigate potential sensitivities.

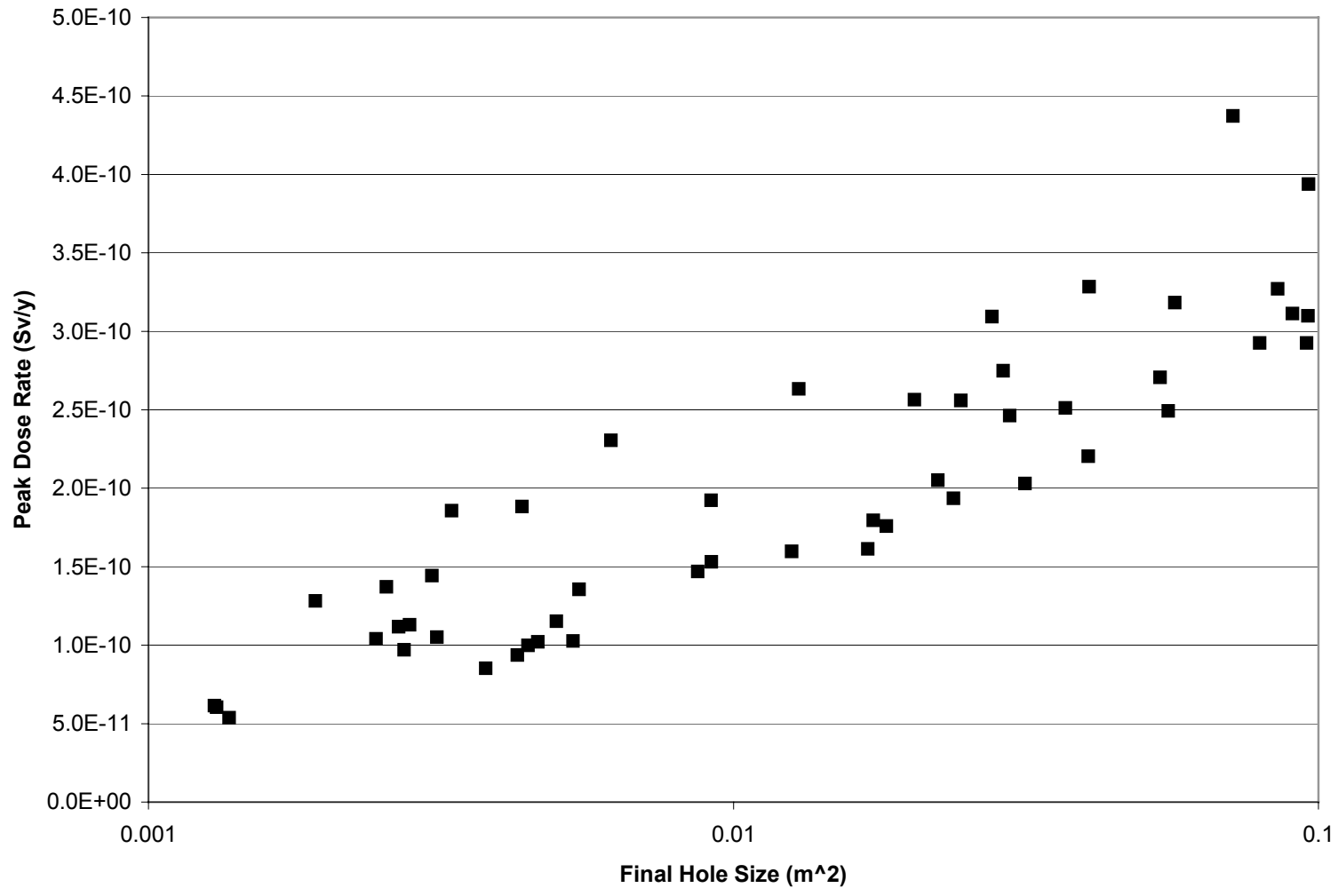


Figure 2.4.1 Variation of Peak Dose with Final Hole Size.



## 3 Case 2: A Simple Probabilistic Test Case

### 3.1 Test Case Specification

The coastal biosphere model described in Section 2.3 provides the basis for this simple probabilistic test case. The parameter probability density functions given in Bergström et al. (1999) referred to in Table 2.3.3 were used to calculate the PDFs of calculated dose and environmental concentrations. Runs were undertaken with 1000 samples.

### 3.2 Intercomparisons

Table 3.1 gives details of some AMBER/Ecolego intercomparisons for individual pathways and for calculations of equilibrium inventories in sediments. The calculated quantities for the sediment inventories are very similar, but not identical. The differences generally appear to be consistent with sampling uncertainties, and these would presumably reduce if a larger number of samples were used. Table 3.2 gives calculations summed over the four consumption pathways for direct comparison with the SKB calculations. In general the agreement with the AMBER and Ecolego calculations is very good; residual differences may be due to the uncertainties associated with the implementation of the algorithms referred to in Section 2.3.

This test case demonstrates the capability of both AMBER and Ecolego to undertake probabilistic calculations. The probabilistic calculations could be used to investigate parameter sensitivities if required. As an example, Figure 3.1 shows how the total dose calculated by AMBER for a unit input from the geosphere of Pu-239 varies with the value of the sediment sorption coefficient. It can be seen that for values of the sorption coefficient towards the bottom of the chosen range there is an overall uncertainty in the calculations of about an order of magnitude (due to uncertainties in other model parameters). There is a general trend for doses to decrease as the sorption coefficient increases (primarily because this results in a more rapid removal of radioactivity from the water column), with the overall uncertainty in the calculated doses also reducing.

**Table 3.1.** AMBER/Ecolego Intercomparisons (*AMBER calculations are in normal font; Ecolego calculations are in italic font*).

Radionuclide	Equilibrium dose rate to Critical Group for a unit input flux of 1 Bq/y: 1%, 50% and 99% values of CDF for each pathway (fish, algae, milk and meat) [Sv/y]	Equilibrium amount in Bay sediments for a unit input flux of 1 Bq/y from the geosphere: 1%, 50% and 99% values of cumulative distribution [Bq]
C-14	1.1E-15, 1.5E-15, 2.2E-15; <i>2.7E-16, 1.2E-15, 2.1E-15</i> 3.9E-20, 2.4E-19, 1.3E-18; <i>4.1E-20, 2.5E-19, 1.5E-18</i> 1.4E-16, 4.5E-16, 1.4E-16; <i>1.2E-17, 3.8E-17, 1.1E-16</i> 1.3E-18, 2.0E-17, 1.3E-16; <i>1.4E-18, 1.6E-17, 1.1E-16</i>	8.5E-7, 7.5E-6, 8.4E-5; <i>6.8E-7, 7.8E-6, 8.7E-5</i>
Cl-36	1.4E-19, 1.1E-18, 7.8E-18; <i>1.5E-19, 1.1E-18, 8.0E-18</i> 3.5E-24, 2.3E-23, 1.9E-22; <i>3.5E-24, 2.8E-23, 2.1E-22</i> 4.6E-17, 1.3E-16, 3.1E-16; <i>4.1E-17, 1.1E-16, 2.4E-16</i> 1.3E-17, 4.2E-17, 1.5E-16; <i>1.1E-17, 3.3E-17, 1.0E-16</i>	8.5E-7, 7.5E-6, 8.4E-5; <i>7.9E-7, 7.9E-6, 9.1E-5</i>
Ni-59	2.8E-18, 1.3E-17, 3.4E-17; <i>2.6E-18, 1.2E-17, 3.3E-17</i> 5.9E-22, 5.0E-21, 3.9E-20; <i>6.8E-22, 5.2E-21, 3.5E-20</i> 9.4E-19, 6.3E-18, 2.8E-17; <i>7.5E-19, 5.2E-18, 2.5E-17</i> 6.6E-20, 6.8E-19, 5.8E-18; <i>6.7E-20, 5.6E-19, 4.4E-18</i>	8.1E-3, 7.8E-2, 6.5E-1; <i>7.2E-3, 7.5E-2, 8.3E-1</i>
Se-79	7.0E-15, 1.3E-14, 2.6E-14; <i>6.8E-15, 1.3E-14, 2.6E-14</i> 1.1E-19, 7.8E-19, 6.0E-18; <i>9.5E-20, 7.4E-19, 6.0E-18</i> 8.6E-18, 8.8E-17, 9.6E-16; <i>7.9E-18, 7.4E-17, 6.9E-16</i> 8.2E-19, 2.1E-17, 1.7E-16; <i>7.7E-19, 2.1E-17, 1.4E-16</i>	5.9 E-3, 2.8E-2, 1.4E-1; <i>4.9 E-3, 3.1E-2, 1.3E-1</i>

Radionuclide	Equilibrium dose rate to Critical Group for a unit input flux of 1 Bq/y: 1%, 50% and 99% values of CDF for each pathway (fish, algae, milk and meat) [Sv/y]	Equilibrium amount in Bay sediments for a unit input flux of 1 Bq/y from the geosphere: 1%, 50% and 99% values of cumulative distribution [Bq]
I-129	1.4E-15, 4.0E-15, 1.1E-14; <i>1.4E-15, 3.8E-15, 1.1E-14</i> 4.3E-18, 3.0E-17, 2.3E-16; <i>3.7E-18, 2.9E-17, 2.1E-16</i> 6.4E-16, 7.0E-15, 4.3E-14; <i>7.2E-16, 5.2E-15, 3.4E-14</i> 1.6E-15, 6.9E-15, 2.3E-14; <i>1.2E-15, 4.9E-15, 1.5E-14</i>	5.6E-4, 2.5E-3, 1.1E-2; <i>5.1E-4, 2.4E-3, 1.3E-2</i>
Cs-135	2.3E-16, 4.6E-16, 1.0E-15; <i>2.4E-16, 4.8E-16, 1.1E-15</i> 3.7E-21, 2.7E-20, 1.9E-19; <i>3.5E-21, 2.7E-20, 2.1E-19</i> 1.4E-17, 9.9E-17, 5.5E-16; <i>1.3E-17, 8.3E-17, 4.9E-16</i> 3.2E-17, 1.5E-16, 5.0E-16; <i>2.8E-17, 1.1E-16, 3.3E-16</i>	8.1E-3, 7.8E-2, 6.5E-1; <i>7.3E-3, 7.4E-2, 7.8E-1</i>
Ra-226	3.7E-15, 1.2E-14, 2.9E-14; <i>3.7E-15, 1.2E-14, 3.0E-14</i> 1.1E-18, 7.2E-18, 5.9E-17; <i>9.9E-19, 7.5E-18, 6.0E-17</i> 1.7E-16, 1.4E-15, 6.0E-15; <i>1.8E-16, 1.2E-15, 5.1E-15</i> 1.9E-16, 7.3E-16, 3.5E-15; <i>1.7E-16, 6.1E-16, 2.9E-15</i>	8.1E-3, 7.8E-2, 6.5E-1; <i>7.0E-3, 7.7E-2, 7.7E-1</i>
Pu-239	1.2E-15, 4.6E-15, 1.2E-14; <i>1.0E-15, 4.9E-15, 1.2E-14</i> 2.0E-18, 1.6E-17, 1.3E-16; <i>1.9E-18, 1.6E-17, 1.3E-16</i> 7.7E-21, 3.8E-19, 5.4E-18; <i>6.3 E-21, 3.7E-19, 3.9E-18</i> 1.3E-19, 3.2E-18, 5.9E-17; <i>1.0E-19, 2.8E-18, 4.9E-17</i>	6.3E-2, 6.6E-1, 4.1E0; <i>7.3E-2, 6.6E-1, 4.0E0</i>

**Table 3.2.** Comparisons with SKB Calculations (*AMBER calculations are in normal font. Ecolego calculations are in italic font. SKB calculations are in bold font*).

Radionuclide	Total equilibrium dose rate to Critical Group for a unit input flux of 1 Bq/y: 1%, 50% and 99% values of CDF [Sv/y]	Radionuclide	Total equilibrium dose rate to Critical Group for a unit input flux of 1 Bq/y: 1%, 50% and 99% values of CDF [Sv/y]
C-14	1.2E-15, 1.6E-15, 2.3E-15 <i>3.1E-16, 1.3E-15, 2.2E-15</i> <b>1.2E-15, 1.7E-15, 2.4E-15</b>	I-129	6.8E-15, 2.0E-14, 6.3E-14 <i>5.5E-15, 1.5E-14, 4.7E-14</i> <b>6.0E-15, 1.8E-14, 5.6E-14</b>
Cl-36	6.6E-17, 1.7E-16, 4.3E-16 <i>5.7E-17, 1.4E-16, 3.3E-16</i> <b>6.3E-17, 1.6E-16, 3.9E-16</b>	Cs-135	3.8E-16, 7.8E-16, 1.5E-15 <i>3.6E-16, 7.2E-16, 1.4E-15</i> <b>3.6E-16, 7.8E-16, 1.5E-15</b>
Ni-59	6.2E-18, 2.2E-17, 5.1E-17 <i>5.3E-18, 2.2E-17, 4.8E-17</i> <b>4.7E-18, 2.2E-17, 5.0E-17</b>	Ra-226	5.3E-15, 1.5E-14, 3.2E-14 <i>5.0E-15, 1.5E-14, 3.2E-14</i> <b>4.9E-15, 1.6E-14, 3.6E-14</b>
Se-79	7.1E-15, 1.3E-14, 2.6E-14 <i>6.9E-15, 1.3E-14, 2.6E-14</i> <b>6.8E-15, 1.4E-14, 2.6E-14</b>	Pu-239	1.2E-15, 4.6E-15, 1.2E-14 <i>1.0E-15, 4.9E-15, 1.2E-14</i> <b>1.5E-15, 6.4E-15, 1.5E-14</b>

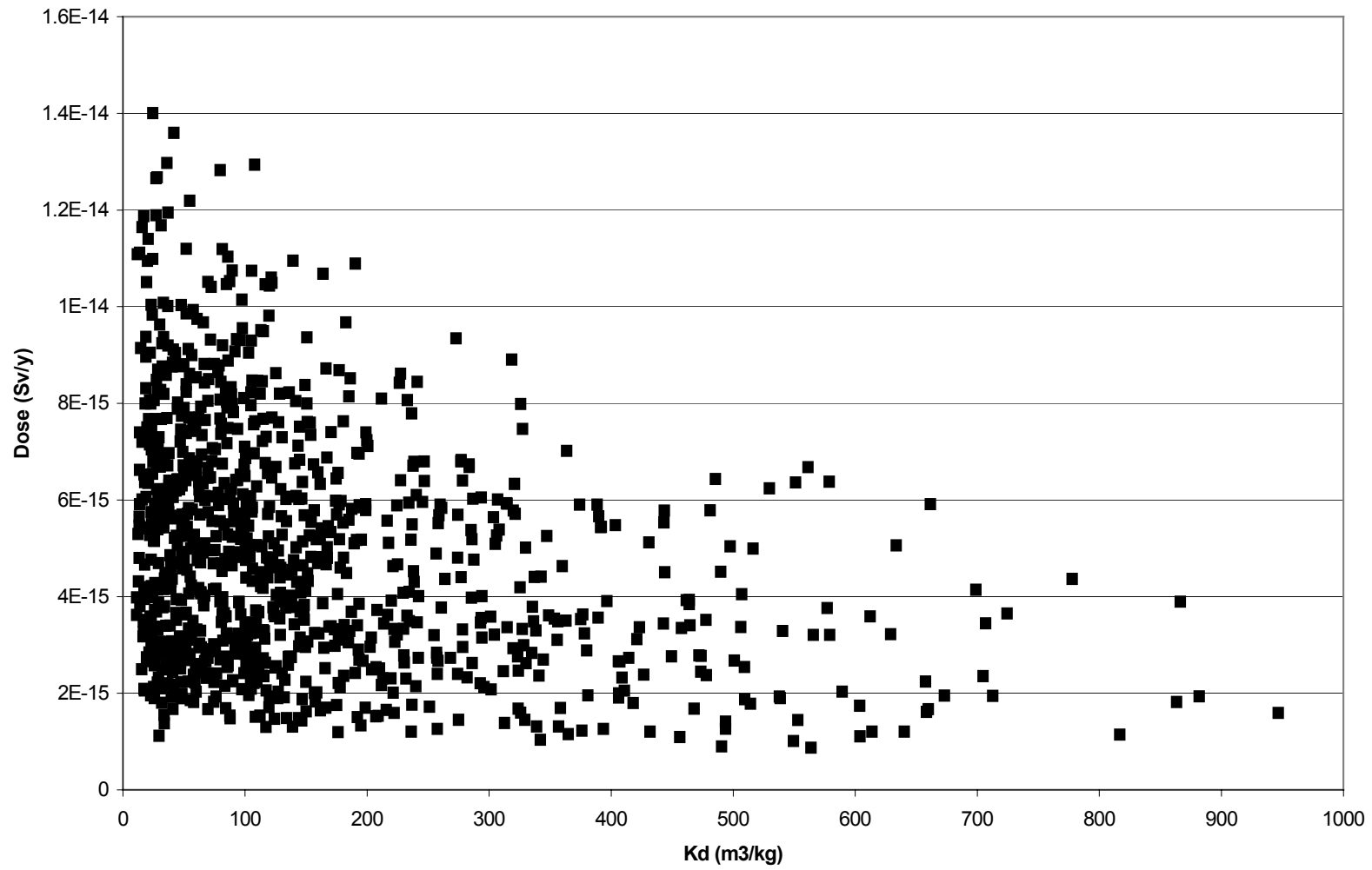


**Figure 3.1.** Dependence of Pu-239 Dose on Sediment  $K_d$ .



## 4 Case 3: Variations on Case 1

### 4.1 Test Case 3.1

#### 4.1.1 Test Case Specification

Case 3.1 has been run with the same parameters as for Case 1, except for the variations given in Table 4.1.1. These parameter variations are not necessarily considered to be realistic values, but enable a wider range of model calculations to be undertaken in order to investigate further any AMBER/Ecolego differences. The continuous variation of the canister hole area was specified in order to provide a test where model the system was changing continuously over most of the simulation period.

**Table 4.1.1:** Parameter Changes for Test Case 3.1.

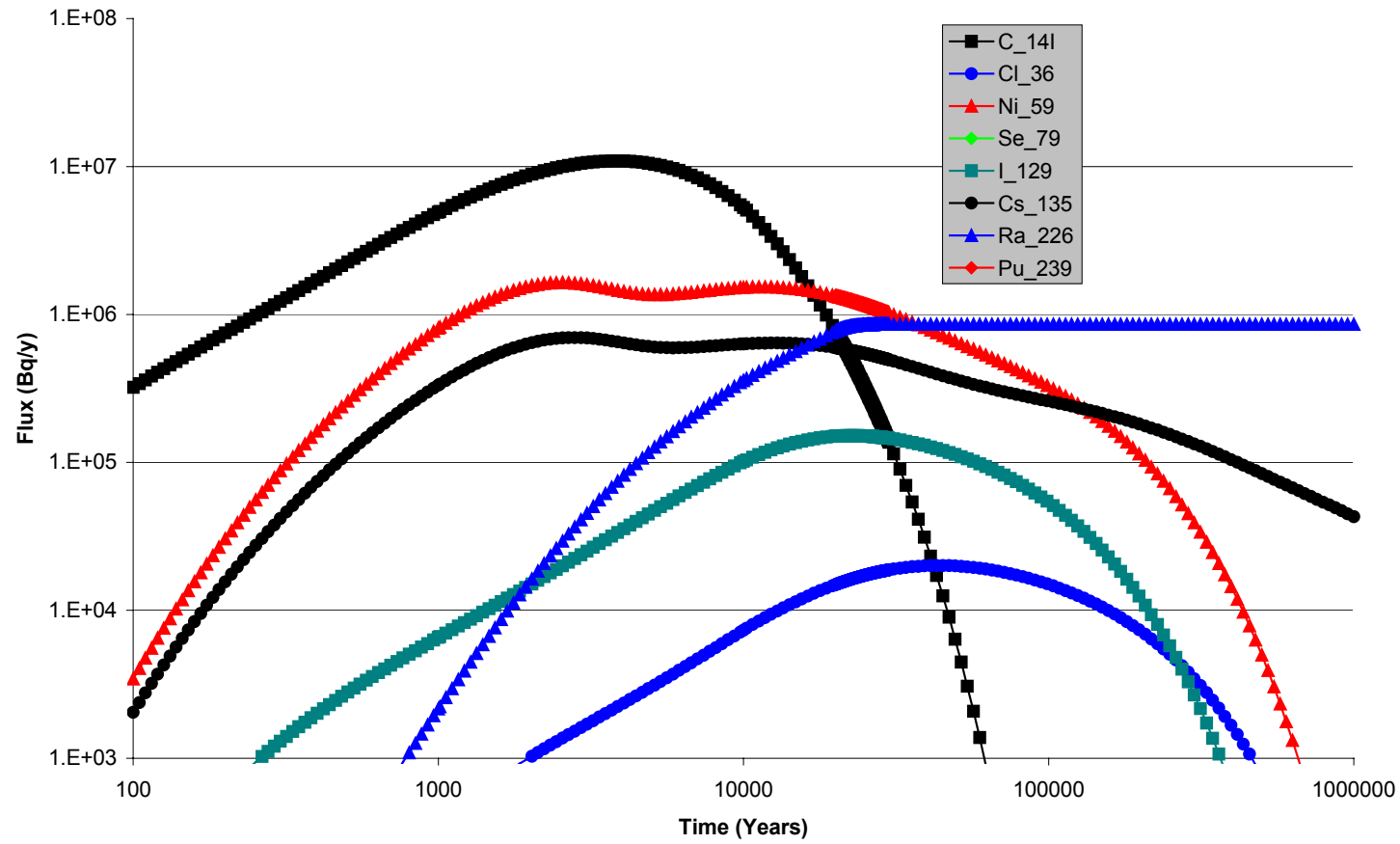
Parameter	Data Source
Instant Release Fractions	1 for all radionuclides- instantaneous availability.
Canister hole area	Varying linearly from 0 to 0.01 m <sup>2</sup> over a period of 10 000 years
Delay time before release commences	0

#### 4.1.2 Intercomparisons

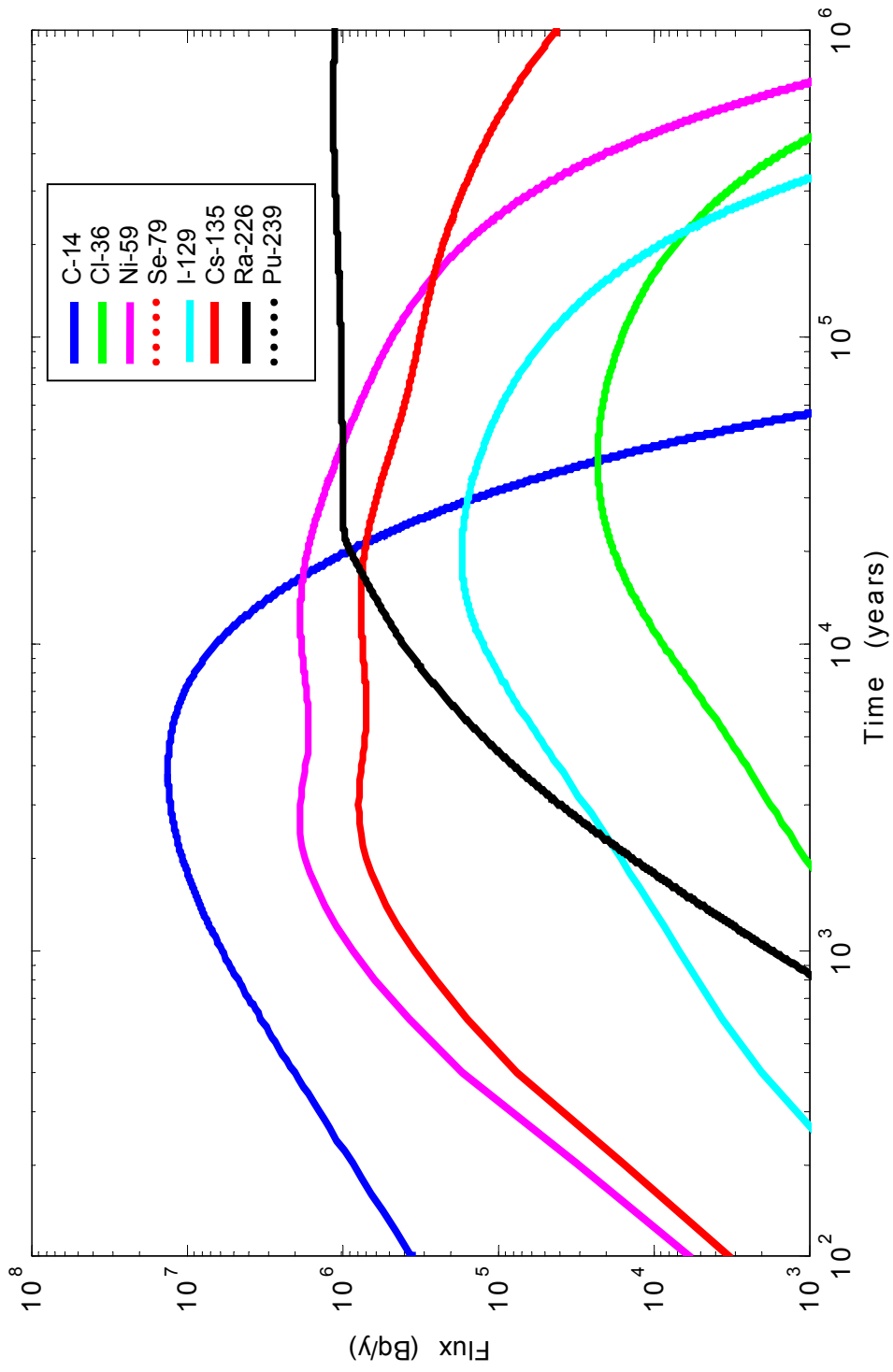
Figure 4.1.1 gives details of the calculated fluxes from the near field calculated by AMBER. Compared with the main deterministic calculations in Section 2 (Figure 2.1.2) it can be seen that peak fluxes are generally higher, and there is now no discontinuity in the flux. The release of radionuclides such as Pu-239 continues to be affected by solubility limitations.

Table 4.1.2 shows comparisons between AMBER and Ecolego for the near field.

The level of agreement between the two sets of calculations is generally similar to that observed for the main test case. If the compartment structure and transfer rates were implemented identically in the two codes one would expect essentially identical results, but it is presumed that there are some (minor) remaining differences in the implementations due to the uncertainties associated with interpreting the SKB near field model.



**Figure 4.1.1a** Fluxes from the Near Field Calculated by AMBER for Test Case 3.1.



**Figure 4.1.1b** Fluxes from the Near Field Calculated by Ecolego for Test Case 3.1.

**Table 4.1.2.** Near-Field Calculations for Test Case 3.1 (*AMBER* calculations are in normal font. *Ecolego* calculations are in italic font).

	Peak flux [Bq y <sup>-1</sup> ] at time [y]	Total flux at 1000 years (and individual fluxes Q1-Q4) [Bq y <sup>-1</sup> ]	Total amount at 1000 years [Bq]	Total flux at 10 000 years (and individual fluxes Q1-Q4) [Bq y <sup>-1</sup> ]	Total amount at 10 000 years [Bq]
C-14	1.1E7 [4.1E3] <i>1.3E7 [3.9E3]</i>	4.9E6 [3.8E6, 1.1E6, 1.2E4, 2.7E2] <i>5.9E6 [4.6E6, 1.4E6, 1.5E4, 2.9E2]</i>	1.6E10 <i>1.7E10</i>	6.2E6 [2.7E6, 2.3E6, 1.2E6, 1.3E4] <i>6.5E6 [2.7E6, 2.4E6, 1.4E6, 1.3E4]</i>	6.1E10 <i>5.7E10</i>
Cl-36	2.0E4[4.1E4] <i>2.3E4[4E4]</i>	3.9E2[3.9E2, 1.1E0, 9.7E-2, 3.5E-4] <i>8.7E3[5.7E3, 1.8E3, 1.2E3, 2.6E0]</i>	9.1E6 <i>9.1E6</i>	8.0E3 [5.1E3, 1.7E3, 1.1E3, 2.8E0] <i>1.6E4 [6.3E3, 5.0E3, 4.4E3, 3.6E2]</i>	2.4E8 <i>2.4E8</i>
Ni-59	1.6E6 [2.6E3] <i>1.9E6 [2.7E3]</i>	8.1E5 [8.1E5, 6.1E2, 3.5E-3, 1.4E-3] <i>8.6E5 [8.6E5, 6.1E2, 3.4E-3, 3.4E-3]</i>	2.1E11 <i>2.1E11</i>	1.5E6 [7.1E5, 8.2E5, 2.0E3, 3.1E1] <i>1.8E6 [8.8E5, 9.5E5, 2.2E3, 2.2E3]</i>	8.1E11 <i>8.1E11</i>
Se-79	6.3E1 [1.0E6] <i>5.8E1 [1.2E5]</i>	7.5E-1 [7.2E-1, 3.8E-2, 1.8E-4, 4.2E-7] <i>9.0E-1 [8.3E-1, 6.4E-2, 4.9E-4, 8.2E-7]</i>	1.2E4 <i>1.4E4</i>	1.6E1 [8.6E0, 6.2E0, 1.7E0, 2.2E-3] <i>1.9E1 [9.8E0, 7.0E0, 2.0E0, 2.1E-3]</i>	4.0E5 <i>3.8E5</i>
I-129	1.6E5 [ 2.0E4] <i>1.7E5 [ 2.0E4]</i>	6.6E3 [6.3E3, 2.2E2, 2.3E1, 4.5E-2] <i>6.8E3 [6.6E3, 2.1E2, 2.3E1, 4.2E-2]</i>	6.3E7 <i>6.2E7</i>	1.1E5 [5.5E4, 3.3E4, 2.5E4, 1.2E2] <i>1.3E5 [3.6E4, 2.7E4, 2.7E4, 1.1E2]</i>	1.4E9 <i>1.3E9</i>
Cs-135	7.0E5 [2.8E3 ] <i>7.8E5 [3.0E3 ]</i>	3.3E5 [3.3E5, 2.3E2, 5.0E-4, 2.3E-3] <i>3.5E5 [3.5E5, 2.3E2, 5.0E-4, 1.2E-3]</i>	4.7E10 <i>4.5E10</i>	6.3E5 [3.3E5, 3.0E5, 2.6E2, 3.0E1] <i>7.4E5 [4.0E5, 3.4E5, 2.9E2, 2.9E1]</i>	2.1E11 <i>2.1E11</i>
Ra-226	8.6E5 [ 2.9E5] <i>1.1E6 [ 5.7E5]</i>	2.2E3 [2.1E3, 1.5E1, 1.4E-4, 8.1E-5] <i>1.7E3 [1.7E3, 1.1E1, 1.1E-4 5.5E-5]</i>	8.3E7 <i>6.1E7</i>	3.6E5 [2.8E5, 7.3E4, 7.6E1, 5.2E0] <i>4.0E5 [3.2E5, 7.9E4, 7.6E1, 4.7E0]</i>	2.4E10 <i>2.3E10</i>
Pu-239	7.1E1 [5.9E4] <i>5.1E1 [3.9E4]</i>	8.1E-5 [8.1E-5, 3.0E-12, 0, 0 ] <i>3.3E-3 [3.3E-3, 1.7E-10, 0, 0 ]</i>	2.3E6 <i>1E7</i>	4.8E0 [4.8E0, 1.4E-6, 0, 0] <i>7.2E0 [7.2E0, 2.7E-6, 0, 0]</i>	1.2E8 <i>1.5E8</i>

## 4.2 Test Case 3.2

### 4.2.1 Test Case Specification

Test Case 3.2 is identical to Test Case 3.1, except that unlimited solubility is assumed for all radionuclides. This variation has been designed to provide a further test comparison for AMBER and Ecolego.

### 4.2.2 Intercomparisons

Figure 4.2.1 give details of the calculated fluxes from the near field. Compared with the calculations for Test Case 3.1, there is no change for five radionuclides that were not subject to solubility limitations (C-14, Cl-36, Ni-59, I-129 and Cs-135). There is a small increase in fluxes from the near field for Ra-226, but the changes for Se-79 and Pu-239 are most marked; the peak flux from the near field for Se-79 has increased by around four orders of magnitude and that for Pu-239 has increased by around five orders of magnitude. This demonstrates very clearly the importance of the choice of the solubility limit parameters for these two radionuclides; in any review of a safety case for a deep repository, the justification for the choice of these parameters would clearly need to be scrutinised.

Table 4.2.1 gives details of comparisons between the AMBER and Ecolego calculations for the radionuclide fluxes that differ from Case 3.1. Again, the key characteristics of the flux profiles for Se-79 and Pu-239 are similarly produced by the two codes, although there remain detailed differences between the two sets of calculations.

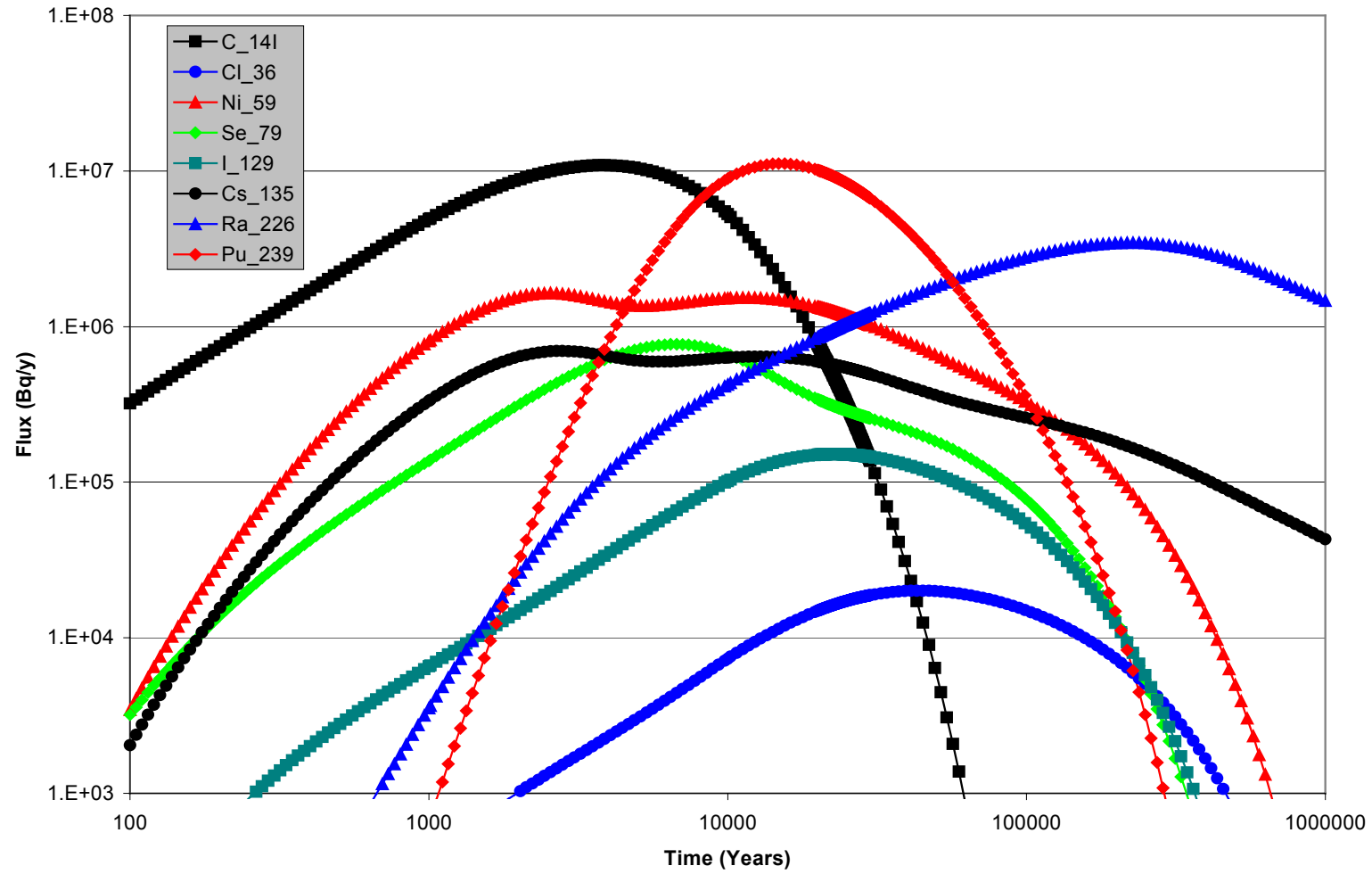
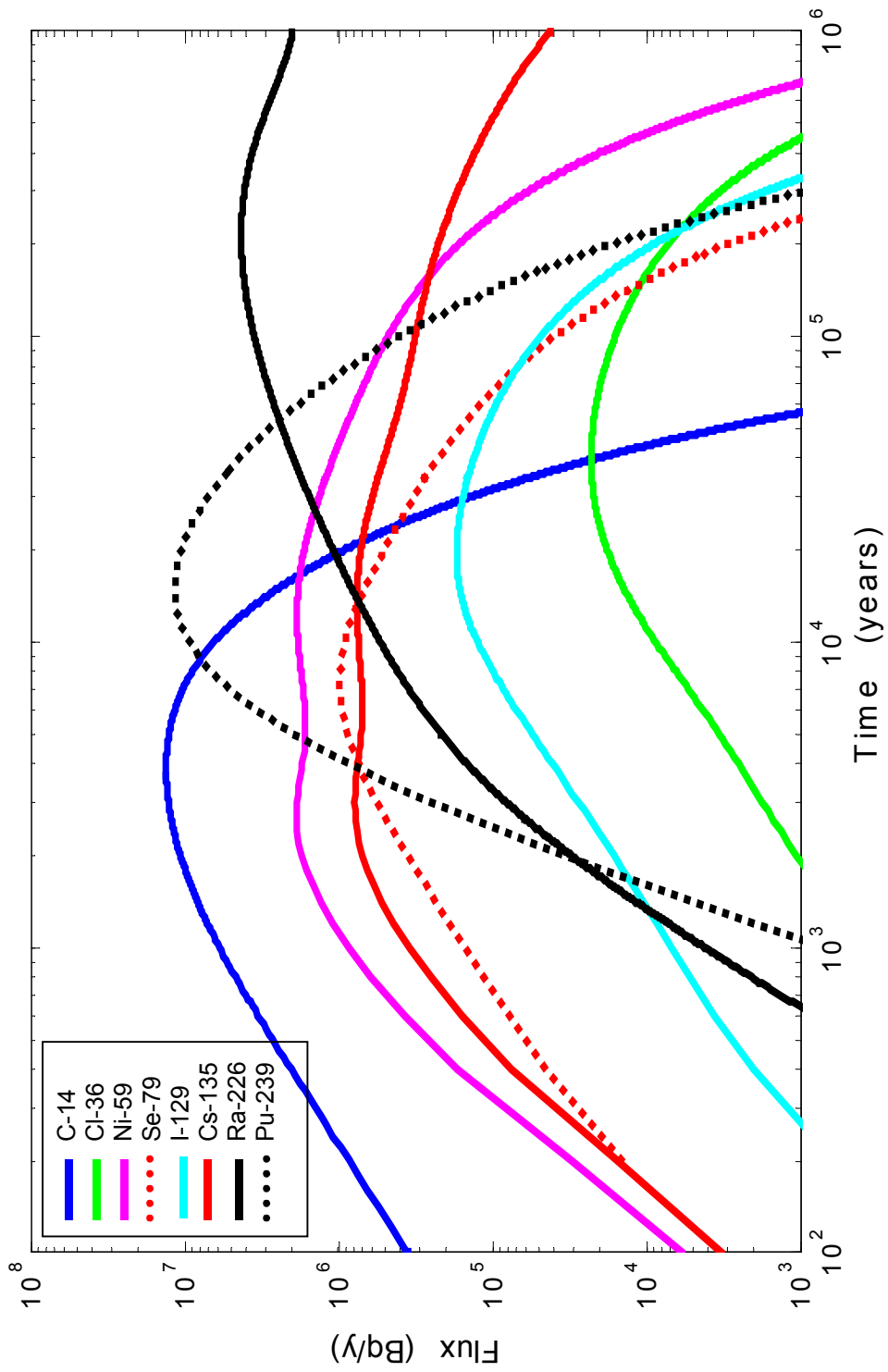


Figure 4.2.1a Fluxes from the Near Field calculated by AMBER for Test Case 3.2.



**Figure 4.2.1b** Fluxes from the Near Field calculated by Ecolego for Test Case 3.2.

**Table 4.2.1.** Near-Field Calculations (*AMBER calculations are in normal font. Ecolego calculations are in italic font*).

	Peak total flux to Geosphere [Bq y <sup>-1</sup> ] and time at which it occurs [y]	Total flux at 1000 years (and individual fluxes Q1-Q4) [Bq y <sup>-1</sup> ]	Total amount in the near-field at 1000 years [Bq]	Total flux at 10 000 years (and individual fluxes Q1-Q4) [Bq y <sup>-1</sup> ]	Total amount in the near-field at 10 000 years [Bq]
Se-79	8.4E5 [7.4E3] <i>9.8E5 [7.5E3]</i>	1.4E5 [1.3E5, 7.1E3, 3.5E1, 7.9E-2] <i>1.5E5 [1.4E5, 7.5E3, 3.7E1, 7.5E-2]</i>	2.3E9 <i>2.3E9</i>	7.9E5 [2.9E5, 3.4E5, 1.5E5, 2.0E2] <i>9.2E5 [3.4E5, 4.0E5, 1.8E5, 2.0E2]</i>	2.1E10 <i>2.0E10</i>
Ra-226	3.5E6 [ 2.3E5] <i>4.3E6 [2.2E5]</i>	3.5E3 [3.5E3, 2.4E1, 2.3E-4, 1.3E-4] <i>4.2E3 [4.1E3, 2.6E1, 2.5E0, 1.3E-4]</i>	1.4E8 <i>1.5E8</i>	4.2E5 [3.3E5, 9.4E4, 1.0E2, 7.0E0] <i>5.3E5 [4.1 E5, 1.1E5, 1.2E2, 7.3E0]</i>	3.0E10 <i>3.1E10</i>
Pu-239	1.1E7 [1.5E4] <i>1.2E7 [1.5E4]</i>	6.5E2 [6.5E2, 2.4E-5, 0, 0 ] <i>7.0E2 [7.0E2, 2.4E-5, 0, 0 ]</i>	1.7E13 <i>1.7E13</i>	8.9E6 [8.9E6, 4.7E0, 0, 0] <i>9.3E6 [9.3E6, 4.8E0, 1.1E-7, 7.4E-6]</i>	7.5E13 <i>7.5E13</i>

## 5 Conclusions

1. Both modelling packages could successfully reproduce SKB's SR 97 calculations for the near field, geosphere and biosphere.
2. The results of the deterministic calculations for the near field and both deterministic and probabilistic calculations for the biosphere, where AMBER and Ecolego used compartment models, were typically in agreement to within one significant figure. The identical results for the calculated equilibrium inventories in Bay sediments illustrate that the calculations by AMBER and Ecolego are essentially the same when the compartment models are identical. The residual differences in the other calculations are due to small differences in the interpretation of the SR 97 models and data.
3. The results of the deterministic calculations for the geosphere, where AMBER used a compartment model and Ecolego a one-dimensional contaminant transport model, were also generally in agreement to within one significant figure, except where radionuclides fluxes are very low (e.g., for  $^{239}\text{Pu}$ ), where the compartmental approximation in AMBER can overestimate the output flux.
4. In several instances the SR 97 documentation was not sufficiently clear to enable the implementation of the models in AMBER and Ecolego to be unambiguous. Examples include the structure of the coastal biosphere model and the algorithms used in some of the dose calculations.
5. Some key issues for the SR 97 assessment have been identified; these provide an indication of where detailed scrutiny will be required of any safety case made by SKB for a deep repository.



## References

- Avilia, R, Broed R. and Pereira, A (2003). Ecolego - a Toolbox for Radioecological Risk Assessments. International Conference on the Protection of the Environment from the Effects of Ionising Radiation, 6 –10 October 2003, Stockholm, Sweden.
- Bergström U, Nordlinder S and Aggeryd I (1999). Models for Dose Assessments: Modules for Various Biosphere Types. SKB report TR-99-14.
- De Hoog, F R, Knight J H and Stokes A N (1982). An Improved Method for Numerical Inversion of Laplace Transforms, *J. Sci. Stat. Comput.*, 3(3), 357-366.
- Enviros QuantiSci and Quintessa Ltd (2002). AMBER version 4.4.
- Hedin A (2002). Integrated Analytic Radionuclide Transport Model for a Spent Nuclear Fuel Repository in Saturated Fractured Rock. *Nuclear Technology* 138 pp 79-205.
- Hodkinson, D P and Maul, P R (1988). 1-D Modelling of Radionuclide Migration through Permeable and Fractured Rock for Arbitrary Length Decay Chains using Numerical Inversion of Laplace Transforms. *Ann. Nucl. Energy*, 15(4), 175.
- Hollenbeck, K J (1998). INVLAP.M: A Matlab Function for Numerical Inversion of Laplace Transforms by the De Hoog Algorithm, <http://www.isva.dtu.dk/staff/karl/invlap.htm>.
- Lindgren M and Widén H (1998). Discretisation in COMP23 for SR 97. SKB report R 98 03.
- Lindgren M and Lindström F (1999). SR 97 Radionuclide Transport Calculations. SKB report TR-99-23.
- Maul P R and Robinson P C (2002). Exploration of Important Issues for the Safety of SFR 1 using Performance Assessment Calculations. To be published as a SKI report.
- Neretkieks I (1979). Transport Mechanisms and Rates of Transport of Radionuclides in the Geosphere as Related to the Swedish KBS Concept. Paper presented to a symposium held in Otaniemi, Finland, 2-6 July 1979. IAEA-SM-243/108.
- Norlinder S, Bergström U and Brittain J (1997). A Generic Dynamic Model of Cs-137 Turnover in Nordic Lakes. *Journal of Environmental Radioactivity* 37 pp 175-191.
- Norlinder S, Bergström U and Mathiasson L (1999). Ecosystem specific dose conversion factors for Aberg, Beberg and Ceberg. SKB report TR-99-15.
- Norman S and Kjellbert N (1990). FARF31 – A Far-field Radionuclide Migration Code for use with the PROPER Package. SKB Report TR 90-01.

Romero L, Moreno L and Neretkieks I (1994). Fast Multiple-Path Model to Calculate Radionuclide Release from the Near Field of a Repository. Nuclear Technology 112, 89-98.

Romero L, Thompson A, Moreno L, Neretkieks I, Widén H and Boghammar A (1999). Comp32/Nucran User's Guide: Proper Version 1.1.6. SKB report R-99-64.

SKB (1999). Deep Repository for Spent Fuel. SR 97- Post-closure safety, volumes I and II. SKB report TR-99-06.

Sudicky, E A and Frind, E O (1982). Contaminant Transport in Fractured Porous Media: Analytical Solutions for a System of Parallel Fractures. Water Resour. Res. 18(6), 1634.

Worgan K J and Robinson P C (1995). The CRYSTAL Geosphere Transport Model, Technical Documentation for Version 2.1. SKI Technical Report 95:55.

Xu, S and Wörman, A (1999). Implications of Sorption Kinetics to Radionuclide Migration in Fractured Rock. Water Resour. Res. 35(11), 3429-3440.